Journal of Solid State Electrochemistry
https://doi.org/10.1007/s10008-024-05932-4

ORIGINAL PAPER

Electrochemical goniometry: keystone reactivity at the three-phase boundary

Thomas S. Varley[1] · **Nathan S. Lawrence**[2] · **Jay D. Wadhawan**[1,2]

Received: 26 April 2024 / Revised: 11 May 2024 / Accepted: 11 May 2024

Abstract
Contact angles of liquid, spherical cap droplets immobilised on an electrode surface and bathed by a fluid are important, quantifiable measures of the liquid/fluid interfacial tension. Optical goniometry, even if computer assisted, suffers when the contact angle is 10° or less. In this work, an alternative method of measurement is considered: electrochemical techniques (voltammetry and chronoamperometry), which rely on the transport of material from within the droplet to the conductive surface. As a result of the reactions that take place at the triple phase boundary, these are demonstrated to provide information on the size and the shape of the droplet, including its contact angle, for the cases when the droplets have a redox analyte and either have a supporting electrolyte, or not. The voltammetric behaviour is seen to change from exhaustive, thin film characteristics, to quasi-steady-state signals as the droplet becomes bigger, or the scan rate becomes larger, or diffusion of the redox material inside the droplet becomes slower. One of the surprising outcomes is that there is a zone of planar diffusion only in the case of the supported droplets, with both the droplet size and its contact angle determining whether this is seen at conventional combinations of scan rates and diffusion coefficients. Experimental data are provided which emphasize key features pertaining to the nature of the redox system and illustrate the facile nature of the contact angle estimation process, albeit to within 10% uncertainty.

Keywords Droplets · Goniometry · Contact angles · Wetting · Diffusional transport

Introduction

The accurate measurement of contact angles (θ) of liquid droplets supported on a surface and bathed by a fluid is an important method for the estimation of the liquid/fluid interfacial tension [1, 2]. Since spreading is driven by the difference in the adhesive work between the liquid and the solid substrate, and the cohesive work required to pull the liquid apart, the contact angle describes the tendency of the liquid to wet the solid substrate and spread [3]. When the contact angle is zero (*viz.* $\theta = 0$), the liquid fully wets the surface, spreading to form a molecularly thin film over the surface; in the exactly opposite scenario, $\theta = \pi$ (180°), full dewetting takes place, and there is no spreading of the liquid droplet over the surface—the droplet retains its spherical nature in what is experimentally realised as "the lotus effect" [4]. Partial wetting occurs when $0 < \theta < \frac{\pi}{2}$, and partial non-wetting takes place when $\frac{\pi}{2} \leq \theta < \pi$. In these last two cases, the shape of the droplet is often considered to be that of a spherical cap [5]. However, experimentally, contact angle goniometry through direct visualisation becomes difficult for $\theta < \frac{\pi}{18}$ (10°). On top of this, it is well-known that static droplet goniometry is often plagued by effects due to solid or liquid contamination, and surface heterogeneity/porosity, which can lead to contact angle pinning [1, 2]. Accordingly, it is desirable to identify alternative methods for the inference of contact angles.

Electrochemical approaches for the determination of the size and shape of liquid droplet deposits on electrode surfaces surrounded by liquid or gaseous media have long been developed [6–10]. These revolve around the notion that the electrochemical timescale can be used as a Polykleitos-type canon, since the spatial extent of the depletion zone close to the electrode surface is a function of the mass transfer

✉ Jay D. Wadhawan
j.wadhawan@hull.ac.uk

[1] Department of Chemistry, The University of Hull, Cottingham Road, Kingston-upon-Hull HU6 7RX, UK

[2] School of Engineering, Chemical Engineering, The University of Hull, Cottingham Road, Kingston-upon-Hull HU6 7RX, UK

Published online: 06 August 2024

coefficient, which itself depends on the experimental timescale: In chronoamperometry, there is an explicit dependence; in voltammetry, this occurs indirectly through the voltage sweep rate. However, although various efforts have been made to model voltammetry of redox compounds in single, or arrays of, droplets on surfaces [11–20], there have been limited successful comparisons with relevant experiments. This is solely due to the complexity of the system, despite its axiosymmetry enabling consideration of the problem in two, rather than three, dimensions. First, there are issues associated with the restricted, two-dimensional spatial nature of the droplet. Second, whilst transport within the droplet can be through diffusion, there are opportunities for ion transfer to couple with electron transfer so that transport of *gegen* (counter) ions in the surrounding fluid may also need to be accounted. Third, the developing charge in the droplet through faradaic reaction requires ionic phase transfer to maintain droplet electroneutrality, which might cause the consideration of increased capacitance in the droplet, together with opportunities for transport through migration, and ohmic losses. Fourth, for the case of a liquid droplet surrounded by a liquid electrolyte, there are possibilities for ion pairing effects [21, 22], the strength of which may be as extreme so as to form a precipitate (in the case of redox compounds dissolved in the droplet), or a new phase (in the case of a redox liquid). Such effects can manifest as a density gradient of redox species inside the droplet, leading to a need to consider natural convection within the droplet. Fifth, for the case of redox surfactants, the concentration gradient resulting from electrolysis can lead to a gradient in the surface tension at the liquid/liquid interface. This can cause Marangoni convection, which may extend into the droplet deposit. Last, there are effects due to an infinite current density at the point at which all three phases (solid surface, liquid droplet and bathing fluid) intersect, owing to the mathematical singularity that exists at that point of contact. This base circumference of the droplet is the three-phase boundary, frequently referred to as the "triple phase junction", or the "triple interface".

The importance of reactivity at the triple phase boundary has been long recognised, with a variety of direct and inferred evidence gathered through optical observations [23–26], precipitation effects [27, 28], footprints from metal deposition [29–31], concentration profilometry [32] and monitoring the changes that take place with increasing the size of the contact line [6, 14, 33, 34], *etc*.—the references do not form an exhaustive list. Moreover, whilst concern has been expressed by some regarding the occurrence of ohmic losses in the vicinity of the growing electrolytic depletion layer inside the droplet [6, 15, 18, 34], and recognises the need for electrolytes to partition into the droplet from the aqueous phase, other work indicates that there is a dominance of behaviour at the three-phase boundary without the requirement for electrolyte partitioning effects to take place [13, 14]. Nevertheless, the consensus is that the electrochemical signature is a function of the droplet size, shape and the mechanism of the electron transfer reaction. As mentioned earlier, the latter is often described as involving a coupled electron/ion phase transfer process [35], due to the macroscopic need to preserve the electroneutrality of the droplet.

However, electrochemical methods to investigate droplet contact angles are limited by the occurrence of electric field effects that induce electrowetting phenomena [36, 37]. Nevertheless, there is a range of droplet systems for which electrowetting does not cause a visible change in the contact angle of droplets ("contact angle saturation"). As demonstrated experimentally, such effects, although not always saturation, can occur around the point of zero charge for the solid/liquid/liquid system [36–40].

In this paper, we examine both chronoamperometry and voltammetry at electroactive droplet-modified electrodes in order to ascertain whether these techniques are able to estimate the contact angles of droplets on surfaces. We utilise experimental systems and limit the potential window to those for which there is no change in the contact angle upon the imposition of an electric field—the droplets are static, so that we can monitor diffusive mass transport contained therein. We do not consider effects outside the droplet. Whilst we have studied liquid nanosystems that span a volumetric range of ten orders of magnitude (from a few tens of yoctolitres [41] to a few tens of femtolitres [42, 43] in previous work, we keep the experiments reported herein confined to a few hundred nanolitres, as these are easier to prepare and visualise experimentally, and we do not have to consider species in non-bulk solvation, as in previous work [44].

Theory

We are interested in the diffusive transport of electroactive species inside a single, sessile liquid droplet resting on a conductive surface, with both the uncovered parts of the surface and the cupola of the droplet bathed by a fluid, as illustrated in Fig. 1. In the experimental work described, this fluid is an aqueous solution of much larger volume than the droplet itself so that the droplet is considered to be under isothermal operation. We ignore both any joule heating of the electrode/droplet/electrolyte interface during electrolysis [45], and the contributions from the heat of the overall electrolysis reaction (the sum of the two electrode reactions). Likewise, because we use dilute concentrations of redox species solubilised in small droplets that face skywards, we assume interfacial tension effects dominate gravity effects [46], and that natural convection driven by density differences in the oxidised and reduced forms of the redox

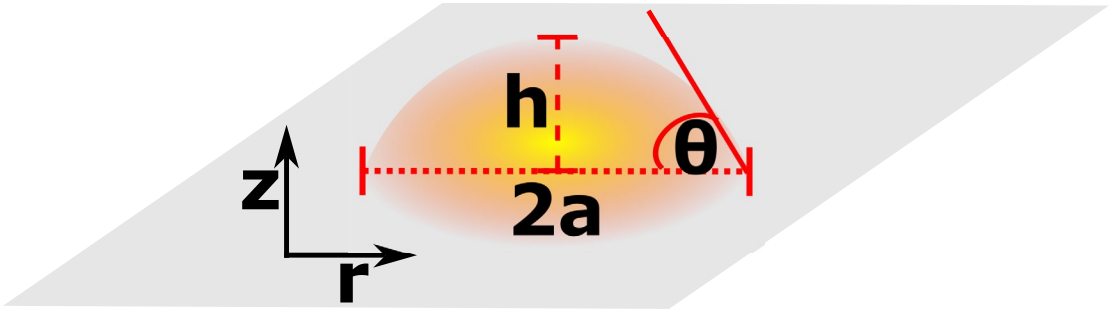

Fig. 1 Illustration of the droplet-modified electrode considered in this work. The droplet is considered to be a spherical cap, of contact radius, a, and height above the electrode surface, h. The liquid/fluid interface exists at the cupola perimeter, and the contact angle, marked as θ, corresponds to the angle subtended by the liquid/fluid interface at the solid surface. The cylindrical, two-dimensional co-ordinate regime (r,z) that is used in this work is illustrated

species is also negligible [47–49]. This is important since the timescales used experimentally are at least one order of magnitude larger than those normally used in electroanalytical chemistry to avoid natural convection effects, and evidence for the occurrence of convection at the three-phase boundary has been reported [14, 50]. In the Results and Discussion section, we will return to this assumption.

Droplet geometry

The droplet is assumed to take up a spherical cap shape, with the dimensions given in Fig. 1. The radius of the equivalent sphere is r_d, with the contact line radius (which corresponds to that of the circular base of the droplet) being a, and with h as the maximum height that the droplet extends above the surface. Although Fig. 1 illustrates the case corresponding to the droplet partially wetting the surface, the equations of the circles describing the liquid/liquid interface for both partially wetting and partially non-wetting droplets are the same, since the two-dimensional co-ordinates of the circle origin are identical (0,h-r_d):

$$x^2 + \left[y - \left(h - r_d\right)\right]^2 = r_d^2 \tag{1}$$

where x refers to the r-direction and y the z-direction. The IUPAC definition of the droplet contact angle, θ, is [51] "the angle between two of the interfaces at the three-phase line of contact", which, as illustrated in Fig. 1, is given in this work as the angle between the droplet and the fluid, extended from the conductive surface from within the droplet. This is identical to the angle subtended at the circle origin to the point at which the drop height is maximum and the three-phase boundary. We recognise the recommended good practice of undertaking analysis of droplet contact angles in the cosine [52], but choose to report experimental data in radian or degrees, for ease of mental visualisation.

Equation (1) can be normalised either through the effective spherical radius of the droplet, r_d, or by the radius of the base circle of the droplet, a:

$$Y = \frac{h}{r_d} - 1 \pm \sqrt{1 - X^2} \tag{2a}$$

$$Z = \frac{h - r_d}{a} \pm \sqrt{\frac{r_d^2}{a^2} - R^2} \tag{2b}$$

in which $X = \frac{x}{r_d}; Y = \frac{y}{r_d}; R = \frac{x}{a}; Z = \frac{y}{a}$. Since we are interested in understanding what occurs at the conductive surface, in this work, we normalise with respect to the radius of the base circle, Eq. (2b). Whilst it is trivial to show that the parameters h and a are readily deduced from knowledge of the sphere radius and contact angle,

$$r_d = \frac{a^2 + h^2}{2h} \tag{3a}$$

$$h = r_d(1 - \cos\theta) \tag{3b}$$

$$a = r_d \sin\theta \tag{3c}$$

practical measurements are easiest if the contact angle is estimated from the diameter of the base circle and the height extended by the droplet above the surface. The ratio between these two variables is a function of the contact angle:

$$h = a(\csc\theta - \cot\theta) \tag{3d}$$

The volume (V_{cap}) and lateral surface area (A_{cap}) of the sessile droplet are readily deduced to be as follows:

$$V_{cap} = \frac{\pi}{6}h\left(h^2 + 3a^2\right) = \frac{\pi}{3}r_d^3(1-\cos\theta)^2(2+\cos\theta) = \frac{\pi}{3}a^3(1-\cos\theta)^2(2+\cos\theta)\csc^3\theta = \frac{\pi}{3}a^3\frac{\sin\theta(2+\cos\theta)}{(1+\cos\theta)^2} \tag{4a}$$

$$A_{cap} = 2\pi r_d h = 2\pi r_d^2(1-\cos\theta) = 2\pi a^2(1-\cos\theta)\csc^2\theta = \frac{2\pi a^2}{(1+\cos\theta)} \tag{4b}$$

Equations (3) and (4) are important for defining the parameters a and h when comparing responses of constant volume droplets at variable contact angle.

Following Lebedev and Sliverman [53], capitalising on the axiosymmetry of the droplet, Amatore et al. [19] proposed the use a conformal transformation of cylindrical co-ordinates (r,z), normalised by the radius of the circular disc in contact with the electrode, into bipolar co-ordinates (ξ,η), a two-dimensional form of toroidal co-ordinates, so as to map the semi-infinite space of the entire electrode/droplet/solution system ($-\infty \le r \le \infty$, $0 \le z \le \infty$) into closed, rectangular space ($-1 \le \xi \le 1$, $-1 \le \eta \le 1$):

$$R = \frac{r}{a} = -\frac{sinh\left\{\frac{\pi}{2}tan\left(\frac{\pi}{2}\eta\right)\right\}}{cosh\left\{\frac{\pi}{2}tan\left(\frac{\pi}{2}\eta\right)\right\} - sin\left(\frac{\pi}{2}\xi\right)} \tag{5a}$$

$$Z = \frac{z}{a} = \frac{cos\left(\frac{\pi}{2}\xi\right)}{cosh\left\{\frac{\pi}{2}tan\left(\frac{\pi}{2}\eta\right)\right\} - sin\left(\frac{\pi}{2}\xi\right)} \tag{5b}$$

This transformation accounts for the space that exists both with the droplet ("inner domain") and that bathing the drop ("outer domain"), as evident from the reported back-transformations [19]:

$$\xi = \frac{2}{\pi}tan^{-1}\left(\frac{2Z}{1-R^2-Z^2}\right) \mp 1 \tag{6a}$$

$$\eta = \frac{2}{\pi}tan^{-1}\left[-\frac{2}{\pi}ln\left\{\frac{\sqrt{(1-R^2-Z^2)^2+4Z^2}}{(1-R)^2+Z^2}\right\}\right] \tag{6b}$$

in which the negative sign in Eq. (6a) refers to the inner domain, whilst the positive sign refers to the outer domain [19]. These co-ordinate transformations enable the key boundaries of the physical model to be identified. Thus, the symmetry axis (reflection plane) of the system through the droplet, $R = 0, 0 \le Z \le \infty$, is transformed to $-1 \le \xi \le 1, \eta = 0$, the bulk solution, taken as $\forall R, Z \to \infty$ corresponds to the single point located at $\xi = 1, \eta = 0$; the curved liquid/liquid interface occurs at $\xi = \frac{2}{\pi}\theta - 1, -1 \le \eta \le 1$ and is represented by a vertical line that separates the droplet and the aqueous domains. This is advantageous as it readily enables for a change in the contact angle of the droplet from partial wetting ($\theta < \pi/2$) to partial non-wetting ($\theta \ge \pi/2$) to be readily computed using finite difference grids, without having to adapt the grid sizing and discretisation pattern to account for a curved boundary. The electrode surface can be fully or partially covered by the oil droplet. As noted by Amatore et al. [19], the portion of the electrode surface that is covered by the droplet, $R \le 1, Z = 0$, is located at $\xi = -1, -1 \le \eta \le 1$, with the bare electrode and insulation that are exposed to the aqueous solution at $R > 1, Z = 0$ occurring at $\frac{2}{\pi}\theta - 1 \le \xi \le 1, \eta = -1$, $\frac{2}{\pi}\theta - 1 \le \xi \le 1, \eta = 1$ and at $\xi = 1, -1 \le \eta \le 1, \eta \ne 0$. Importantly, the three-phase boundary—the circular point of contact between the solid electrode and the two liquids, occurs at $-1 \le \xi \le \frac{2}{\pi}\theta - 1, \eta = -1$ and $-1 \le \xi \le \frac{2}{\pi}\theta - 1, \eta = 1$ from within droplet. Thus, in this formulation, inasmuch as the transform provides a discontinuity at $\eta = \pm 1$, it enables the three-phase boundary to be modelled as a thin volume torus, with a wedge-type cross-section, so that in practice, $\eta_{min} = -0.86$ affords an error that can be considered to be negligible [19].

We recognise that this is a versatile system and can account for the case where the electrode is not fully covered by the droplet, through defining the cut-off points for the electrode and its housing insulation.

Transport equations and boundary conditions

Transport within the droplet is assumed to occur through diffusion of the redox analyte only. Accordingly, Fick's second law expressed in terms of cylindrical co-ordinates:

$$\frac{\partial c}{\partial \tau} = \frac{\partial^2 c}{\partial R^2} + \frac{1}{R}\frac{\partial c}{\partial R} + \frac{\partial^2 c}{\partial Z^2} \tag{7}$$

in which $c = \frac{c}{c_0}$ is the concentration of the redox species (C) normalised by its initial value, c_0, and $\tau = \frac{Dt}{a^2}$ is the reduced time variable—the Fourier number for mass transport, with D being the diffusion coefficient of the redox species, and t the real time, needs to be transformed into the toroidal space of Eq. (5). Changing the variables results in the following expressions, which enable the conversion of transport equations from (R,Z) space into [ξ,η] co-ordinates.

$$\frac{\partial}{\partial R} = -\frac{2}{\pi}\cos\left(\frac{\pi}{2}\xi\right)\sinh\left\{\frac{\pi}{2}\tan\left(\frac{\pi}{2}\eta\right)\right\}\frac{\partial}{\partial \xi} + \frac{4}{\pi^2}\cos^2\left(\frac{\pi}{2}\eta\right)\left[\sin\left(\frac{\pi}{2}\xi\right)\cosh\left\{\frac{\pi}{2}\tan\left(\frac{\pi}{2}\eta\right)\right\} - 1\right]\frac{\partial}{\partial \eta} \tag{8a}$$

$$\frac{\partial}{\partial Z} = -\frac{2}{\pi}\left[\sin\left(\frac{\pi}{2}\xi\right)\cosh\left\{\frac{\pi}{2}\tan\left(\frac{\pi}{2}\eta\right)\right\} - 1\right] \frac{\partial}{\partial \xi} - \frac{4}{\pi^2}\cos^2\left(\frac{\pi}{2}\xi\right)\cos\left(\frac{\pi}{2}\eta\right)\sinh\left\{\frac{\pi}{2}\tan\left(\frac{\pi}{2}\eta\right)\right\}\frac{\partial}{\partial \eta} \tag{8b}$$

Hence, considering $\frac{\partial^2}{\partial R^2} = \frac{\partial}{\partial R}\left(\frac{\partial}{\partial R}\right)$ and $\frac{\partial^2}{\partial Z^2} = \frac{\partial}{\partial Z}\left(\frac{\partial}{\partial Z}\right)$, the two-dimensional Laplacian operator in cylindrical co-ordinates is reformulated as given in Eq. (9):

$$\frac{\partial^2}{\partial R^2} + \frac{1}{R}\frac{\partial}{\partial R} + \frac{\partial^2}{\partial Z^2} = \Delta\left(\frac{\partial^2}{\partial \xi^2} + \alpha\frac{\partial^2}{\partial \eta^2} - \beta\frac{\partial}{\partial \eta}\right) + \Lambda\left(\gamma\frac{\partial}{\partial \xi} - \delta\frac{\partial}{\partial \eta}\right) \tag{9}$$

where,

$$\frac{\pi^2}{4}\Delta = \left[cosh\left\{\frac{\pi}{2}tan\left(\frac{\pi}{2}\eta\right)\right\} - sin\left(\frac{\pi}{2}\xi\right)\right]^2$$

$$\frac{\pi^2}{4}\alpha = cos^4\left(\frac{\pi}{2}\eta\right)$$

$$\frac{\pi}{2}\beta = sin(\pi\eta)cos^2\left(\frac{\pi}{2}\eta\right)$$

$$\Lambda = \sqrt{\Delta}$$

$$\gamma = cos\left(\frac{\pi}{2}\xi\right)$$

$$\frac{\pi}{2}\delta = cos^2\left(\frac{\pi}{2}\eta\right)\left[sin\left(\frac{\pi}{2}\xi\right)coth\left\{\frac{\pi}{2}tan\left(\frac{\pi}{2}\eta\right)\right\} - csch\left\{\frac{\pi}{2}tan\left(\frac{\pi}{2}\eta\right)\right\}\right]$$

In order to test the expression for the operator given in Eq. (9), the problem of transport-limited current at a microdisc electrode was considered, for a contact angle of zero [54]. This outputted the anticipated results: after a small, short-time artefact, the Aoki-Osteryoung [55] and Shoup-Szabo [56] equations (with numerical correction to account for the differences in the definitions of the normalised time variables) were followed for their relevant time domains (data not shown).

We are interested in both the chronoamperometric and voltammetric response when a liquid droplet is either electrochemically supported, or unsupported, and, in both cases, bathed by a fully electrochemically supported liquid solution, and in how these change with contact angle. Accordingly, we capitalise on the axiosymmetry of the system (around $Z = 0$, and equivalently, $\eta = 0$) and only simulate transport in the droplet, *viz.* in the domain $-1 \le \xi \le \frac{2}{\pi}\theta - 1, -0.86 \le \eta \le 0$ (see Fig. 2), which corresponds to the space that has already been considered by Amatore and co-workers [19]. This means that we make the assumption that transport of counter ions in the aqueous phase and their phase transfer kinetics do not affect the electrochemical response. As in the earlier work by Compton and co-workers on hemispherical droplets [13, 14], we make two further assumptions: first, of electrochemical reversibility of the electrode reaction, treated as $A - e^- \leftrightarrows B$ (*viz.* fast electrode kinetics), and, second, that the diffusion coefficients of species A and B are equal. Additionally, we only consider the forward voltammetric potential sweep, corresponding to the oxidation of species A (treated so that its dimensionless concentration is c).

In the case of the chronoamperometry experiments, the transport equation is as follows:

$$\frac{\partial c}{\partial \tau} = \Delta\left(\frac{\partial^2 c}{\partial \xi^2} + \alpha\frac{\partial^2 c}{\partial \eta^2} - \beta\frac{\partial c}{\partial \eta}\right) + \Lambda\left(\gamma\frac{\partial c}{\partial \xi} - \delta\frac{\partial c}{\partial \eta}\right) \tag{10a}$$

whilst for linear sweep voltammetry, it is given as follows:

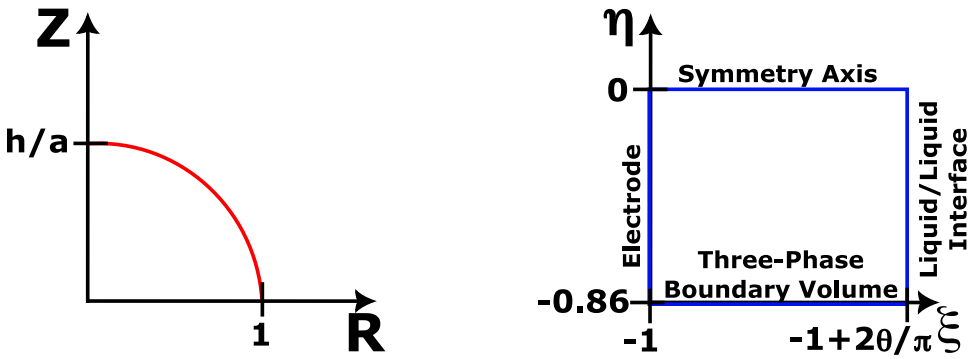

Fig. 2 The spatial domain simulated in this work in R,Z space (left) and in transformed space (right). Note that the symmetry axis is the reflection plane, for the other half of the droplet, and the line at η = -0.86 marks the start of the wedge-type torus that defines the outer-most surface of three-phase boundary volume that faces towards the bulk of the droplet

Table 1 Boundary conditions for the four cases considered in this work[a]

Spatial Area/ Time	Case I: CA, unsupported	Case II: CA, supported	Case III: LSV, unsupported	Case IV: LSV, supported
Initial conditions	$\tau \le 0, c = 1, -1 \le \xi \le \frac{2}{\pi}\theta$ $-1, -0.86 \le \eta \le 0$	$\tau \le 0, c = 1, -1 \le \xi \le \frac{2}{\pi}\theta$ $-1, -0.86 \le \eta \le 0$	$\varepsilon \le u, c = 1, -1 \le \xi \le \frac{2}{\pi}\theta$ $-1, -0.86 \le \eta \le 0$	$\varepsilon \le u, c = 1, -1 \le \xi \le \frac{2}{\pi}\theta - 1, -0.86 \le \eta \le 0$
Electrode surface	$\tau > 0, c = 0, -1 \le \xi \le \frac{2}{\pi}\theta - 1,$ $\eta = -0.86; \left(\frac{\partial c}{\partial \xi}\right)_{\xi=-1,\forall\eta,} = 0$	$\tau > 0, c = 0, -1 \le \xi \le \frac{2}{\pi}\theta - 1,$ $\eta = -0.86; c = 0, \xi = -1, \forall\eta$	$\varepsilon > u, c = (1+e^{\varepsilon})^{-1}, -1 \le \xi \le \frac{2}{\pi}\theta - 1,$ $\eta = -0.86; \left(\frac{\partial c}{\partial \xi}\right)_{\xi=-1,\forall\eta} = 0$	$\varepsilon > u, c = (1+e^{\varepsilon})^{-1}, -1 \le \xi \le \frac{2}{\pi}\theta - 1,$ $\eta = -0.86; c = (1+e^{\varepsilon})^{-1}, \xi = -1, \forall\eta$
Liquid | liquid interface	$\tau > 0, \left(\frac{\partial c}{\partial \xi}\right)_{\xi=\frac{2}{\pi}\theta-1,\forall\eta} = 0$	$\tau > 0, \left(\frac{\partial c}{\partial \xi}\right)_{\xi=\frac{2}{\pi}\theta-1,\forall\eta} = 0$	$\varepsilon > u, \left(\frac{\partial c}{\partial \xi}\right)_{\xi=\frac{2}{\pi}\theta-1,\forall\eta} = 0$	$\varepsilon > u, \left(\frac{\partial c}{\partial \xi}\right)_{\xi=\frac{2}{\pi}\theta-1,\forall\eta} = 0$
Axis of reflection	$\tau > 0, \left(\frac{\partial c}{\partial \eta}\right)_{\forall\xi,\eta=0} = 0$	$\tau > 0, \left(\frac{\partial c}{\partial \eta}\right)_{\forall\xi,\eta=0} = 0$	$\varepsilon > u, \left(\frac{\partial c}{\partial \eta}\right)_{\forall\xi,\eta=0} = 0$	$\varepsilon > u, \left(\frac{\partial c}{\partial \eta}\right)_{\forall\xi,\eta=0} = 0$

CA chronoamperometry, *LSV* linear sweep voltammetry

[a]Supported/unsupported refer to whether the droplet contains supporting electrolyte or not

$$p^2\frac{\partial c}{\partial \varepsilon} = \Delta\left(\frac{\partial^2 c}{\partial \xi^2} + \alpha\frac{\partial^2 c}{\partial \eta^2} - \beta\frac{\partial c}{\partial \eta}\right) + \Lambda\left(\gamma\frac{\partial c}{\partial \xi} - \delta\frac{\partial c}{\partial \eta}\right) \tag{10b}$$

in which the a dimensional potential is $\varepsilon = \frac{F}{RT}\left(E - E^{0\prime}\right) = \frac{F}{RT}\left(E - E^{0\prime}\right) + \frac{F}{RT}vt$, where F is the Faraday constant (96,485.3 C mol^{-1}), R is the molar gas constant (8.3145 J mol^{-1} K^{-1}), T is the absolute temperature, E is the applied potential difference, E_i is the starting potential so that the dimensionless starting potential, $u = \varepsilon_i = \frac{F}{RT}\left(E - E^{0\prime}\right)$, and $E^{0'}$ is the formal potential for the A/B redox couple. The normalised spatio-temporal variable p is given by $p = a\sqrt{\frac{Fv}{DRT}}$, where v is the voltage scan rate, so that p^2 represents the reduced scan rate, $p^2 = \frac{d\varepsilon}{d\tau}$, and $\frac{1}{p^2}$ is the voltammetric Fourier number.

The relevant boundary conditions for each of the four cases considered are outlined in Table 1. Note that in this work, in contrast to earlier hemispherical models [13], we treat supported droplets with an *active* three-phase boundary.

Current evaluation

The current comprises contributions from both the main electrode situated at $\xi = -1$, $-0.86 \le \eta \le 0$, and that at the three-phase boundary, which is located at $-1 \le \xi \le (2/\pi)\theta - 1$, $\eta = -0.86$. In the case of the unsupported droplet, the contribution from the former is zero, owing to the Neumann boundary condition that is imposed there. Thus, in general, the total current (i) flowing is given by the following:

$$\frac{i}{F} = \frac{i_{main}}{F} + \frac{i_{tpb}}{F} = \int j_{main}\,dS_{main} + \int j_{tpb}\,dS_{tpb} \tag{11}$$

where j is the flux of material to the electrode surface and S is the area of the active interface, and the subscripts main and tpb refer to the main electrode and the three-phase boundary, respectively.

For cases I and III, where the droplet is unsupported, S is the curved surface area of the wedge-type torus volume, for which the length is effectively the circumference of the droplet ($2\pi a$), and the curved width is the sector length ($r_{ring}\theta$) that is dependent on the contact angle and length of the three-phase boundary (r_{ring}). The latter is determined by the hemispherical nature of the active interface, and it is readily demonstrable that [19] $r_{ring} \approx a\left|csch\left\{\frac{\pi}{2}tan\left(\frac{\pi}{2}\eta_{min}\right)\right\}\right|$, *viz.* a constant that depends on both the base size of the droplet, and the minimum value of η for an acceptable error. The ratio r_{ring}/a affords to $\eta_{min} = -0.86$ corresponds to a three-phase boundary width that is merely *ca.* 2‰ of droplet basal radius. This is a value that is

very similar to that employed by Fisher et al. for boundary method simulations of the triple phase junction at hemispherical droplets [13]. Thus, in real space, for droplets that have a ~ 0.1 mm, setting η_{min} = -0.86 corresponds to a maximum three-phase boundary width of 0.2 μm; likewise, setting a ~ 0.5 mm affords a maximum three-phase boundary width of ~ 0.9 μm. These values are smaller than those inferred experimentally by Compton et al. through electrochemical deposition of metals in and array of unsupported water droplets (~ 2 μm) for the first case [30], or by Chen and Sato [57], who approximated the observed steady-state voltammetry of ferrocene in single, unsupported polymeric oil droplets as though being derived from microband electrode, of width ~ 9–18 μm in the second case. This difference is not an issue, since the electrolysis timescales impact on the observed effective widths, whilst the region of space that is the singularity will be much smaller. Hence, $dS_{tbp} = 2\pi a^2 \left| csch\left\{ \frac{\pi}{2} tan\left(\frac{\pi}{2} \eta_{min} \right) \right\} \right| d\theta$. Owing to the nature of the mapping transform used in Eq. (5), the perpendicular flux of material to the arc that forms the beginning of three-phase boundary volume occurs in two-dimensions, $j_{tpb} = -\frac{Dc_0}{a} \sqrt{\left(\frac{\partial c}{\partial R} \right)^2_{tpb} + \left(\frac{\partial c}{\partial Z} \right)^2_{tpb}}$. Thus, for Cases I and III, using the expressions given in Eq. (8), the dimensionless current at the three-phase boundary, ψ_{tpb}, is given by Eq. (12) below:

$$\begin{aligned} \psi_{tpb} &= \frac{i_{tpb}}{2\pi FDac_0} \\ &= -\frac{4}{\pi^2}\theta \cos^2\left(\frac{\pi}{2}\eta_{min}\right) \left| \operatorname{csch}\left\{ \frac{\pi}{2} \tan \left(\frac{\pi}{2}\eta_{min} \right) \right\} \right| \left[\cosh\left\{ \frac{\pi}{2} \tan\left(\frac{\pi}{2}\eta_{min} \right) \right\} \right. \\ &\quad \left. -\sin\left(\frac{\pi}{2}\xi \right) \right] \left(\frac{\partial c}{\partial \eta} \right)_{\eta=\eta_{min}} \end{aligned} \tag{12}$$

where the integral has been taken from θ = 0 to θ. The current at the three-phase boundary thus is proportional to the product of the contact line size (2πa) and the contact angle (θ) of the droplet, in addition to the diffusivity and concentration of the redox species contained within the liquid droplet. Thus, for unsupported droplets, Eq. (12) replaces Eq. (11) to express the total dimensionless current (ψ). Note that this model is different to that proposed by Fisher and co-workers [13], since the boundary condition imposed at the liquid/liquid in their model is one-dimensional in cylindrical co-ordinates, whilst it is two-dimensional in this work. This means that *qualitative* and not quantitative wave-shape comparisons may be made between voltammograms produced from these two approaches.

For Cases II and IV, the electrode reaction takes place at both the three-phase boundary and the main electrode. Thus, since the contact area is $S_{main} = \pi a^2$, and the perpendicular flux of material to the electrode is $j_{main} = -D\left(\frac{\partial C}{\partial z} \right)_{z=0}$, the current through the main surface is identical to that at a microdisc electrode, *viz.* $j_{main} = -D\left(\frac{\partial C}{\partial z} \right)_{z=0}$ RdR. Thus, since we curtail the main electrode at $\eta = \eta_{min}$ = -0.86, under the transformation given in Eq. (5), and using Eq. (8), the dimensionless current at the main electrode is given by Eq. (13) below:

$$\begin{aligned} \psi_{main} &= \frac{i_{main}}{2\pi FDac_0} \\ &= -\frac{\pi}{2} \int_{\eta=\eta_{min}}^{0} \frac{sec^2\left(\frac{\pi}{2}\eta\right) sinh\left\{ \frac{\pi}{2} tan\left(\frac{\pi}{2}\eta \right) \right\}}{cosh\left\{ \frac{\pi}{2} tan\left(\frac{\pi}{2}\eta \right) \right\} + 1} \left(\frac{\partial c}{\partial \xi} \right)_{\xi=-1} d\eta \end{aligned} \tag{13}$$

This expression is independent of the contact angle, but depends on the contact line size, together with the diffusivity and concentration of the redox species contained within the droplet. Thus, for supported droplets, Eq. (11) is replaced by Eq. (14), to yield a total current that is dependent on both the size and, thanks to the three-phase boundary effect, the shape of the spherically capped droplet:

$$\psi = \psi_{main} + \psi_{main} \tag{14}$$

in which $\psi = \frac{i}{2\pi FDac_0}$. Note that this is different to the model reported by Fisher and co-workers [13], where the three-phase boundary maintained a no-flux boundary condition whilst faradaic reactions occurred at the main electrode.

Hence, it would appear that, in both chronoamperometric and voltammetric experiments, the observed total current at a single liquid droplet that is either supported or unsupported should suffice to afford an electrochemical goniometric measurement.

Fractional conversion of the droplets

The charge (q) passed during the electrolysis of oil droplets is an alternative route to droplet goniometry, since, for a one-electron exhaustive electrolysis, Faraday's laws and Eq. (4) afford $q_0 = Fc_0V_{cap} = \frac{\pi}{3}Fa^3c_0 \frac{\sin\theta(2+\cos\theta)}{(1+\cos\theta)^2}$. Thus, the fractional extent of the electrochemical conversion of the droplet, $\Omega = \frac{q}{q_0}$, also depends on the droplet contact angle, as well as the integral of the current/time or current/voltage curves. The monitoring of these not only provides a useful validation of the simulation [58], but can be used experimentally to ascertain the inference of multi-electron reactions occurring within the droplets [43, 59–65], or redox catalysis at the liquid/liquid interface [25, 42, 66–74]. Thus, for chronoamperometry:

$$\int \psi \mathrm{d}\tau = \frac{\Omega}{6}\left(\frac{\sin\theta(2+\cos\theta)}{(1+\cos\theta)^2}\right) \tag{15a}$$

and for linear sweep voltammetry:

$$\int \psi \mathrm{d}\varepsilon = \frac{\Omega}{6}\mathrm{p}^2\frac{\sin\theta(2+\cos\theta)}{(1+\cos\theta)^2} \tag{15b}$$

These expressions are valid, irrespective of whether the droplet is electrochemically supported or unsupported. Further, Eq. (15b) indicates that, all other things being constant, thin layer voltammetric behaviour takes place at smaller voltage scan rates, as observed experimentally [14, 21, 23, 29, 30, 75–87].

Computational methods

Numerical simulation was undertaken via program encoding in GNU FORTRAN using the freely available gfortran compiler, with double-precision variables. These were executed on a MacBook Air computer running with a 1.3 GHz Intel Core i5 processor, with 4 GB of DDR3 RAM at 1600 MHz speed. These simulations employed a finite difference spatial grid involving 100×100 nodes, using centred differences for spatial terms and forward differences for temporal gradients. The Peaceman-Rachford alternating direction implicit method was used to solve the transport equations [88]. Instabilities in the simulations resulting from this method [89] were, in most cases, overcome through the use of small time/potential increments, but keeping them as large as possible to reduce simulation time, and without adversely affecting numerical convergence. Currents were calculated through trapezoidal quadrature. Note that in Cases I and III, we followed the recommended practice [19] of averaging the reduced current over the entire length of the three-phase boundary arc.

For chronoamperometric transients, an expanding temporal grid was employed [90], after an initial uniform time step, so as to assist in reducing the oscillations of the method and improve simulation timescales. For unsupported droplets (Case I), transients were calculated for a reduced timescale $\tau=10$, with the initial time step being $\mathrm{d}\tau_0=10^{-6}$ and used up to a threshold time $\tau_0=10^{-3}$, after which time step expansion occurred with the expansion factor being $\omega=5\times10^{-5}$. For supported droplets (Case III), a similar process was used, but with the following parameters: $\tau=1$, $\mathrm{d}\tau_0=10^{-9}$, $\tau_0=10^{-6}$ and $\omega=5\times10^{-5}$. In contrast, the potential change was maintained uniformly at $\Delta\varepsilon=10^{-4}$ in all voltammetric simulations, with a dimensionless potential range of 20.

Single simulations of chronoamperometry transients took *ca.* 650 s for Case I, and 1200 s for Case II; single linear sweep voltammograms took *ca.* 1000 s computing time for both Case III and Case IV. Data were imported using Matlab R2019b (Mathworks) for graphical processing.

Theoretical results and discussion

Chronoamperometric transients for the oxidation of supported and unsupported droplets (Cases I and II) are illustrated in Fig. 3 at three different contact angles, corresponding to partially wetting ($\theta=\pi/4$), hemispherical ($\theta=\pi/2$) and partially non-wetting ($\theta=3\pi/4$) droplets. The data for Case I match-up with those reported previously [19], verifying the quality of the simulation. In all cases, after a very short transient artefact (up to *ca.* $\tau=10^{-5}$), the current decays in the manner anticipated for diffusion, with a gradient that is independent of the contact angle. Eventually, typically around $\tau=1$ (for unsupported droplets), or sooner (for supported droplets), the effects of the restricted environment result in the current rapid tailing off, resulting in exhaustive electrolysis. As expected, for a fixed electrolysis time, the more wetting the droplet is, the greater is the degree of oxidation, and the sooner is the occurrence of the rapid decay in current.

This general picture is more dramatic in the case of the supported droplets (Case II) compared with the unsupported droplets (Case I), for which the currents are higher, owing to the large surface area where the heterogeneous oxidation can take place. In these supported droplets, the initial current decay is Cottrellian, and independent of the droplet

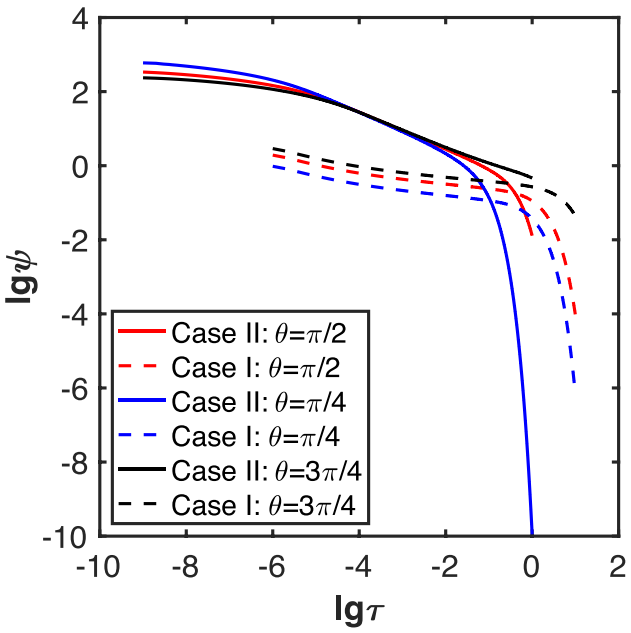

Fig. 3 Chronoamperometric transients corresponding to transport-limited electrolysis at an electrode modified with a single droplet that contains (Case II, solid lines), and does not include (Case I, dashed lines) supporting electrolyte. The results from three contact angles, corresponding to partially wetting droplets ($\theta=45°$, blue), partially non-wetting droplets ($\theta=135°$, black) and hemispherical droplets ($\theta=90°$, red), are given

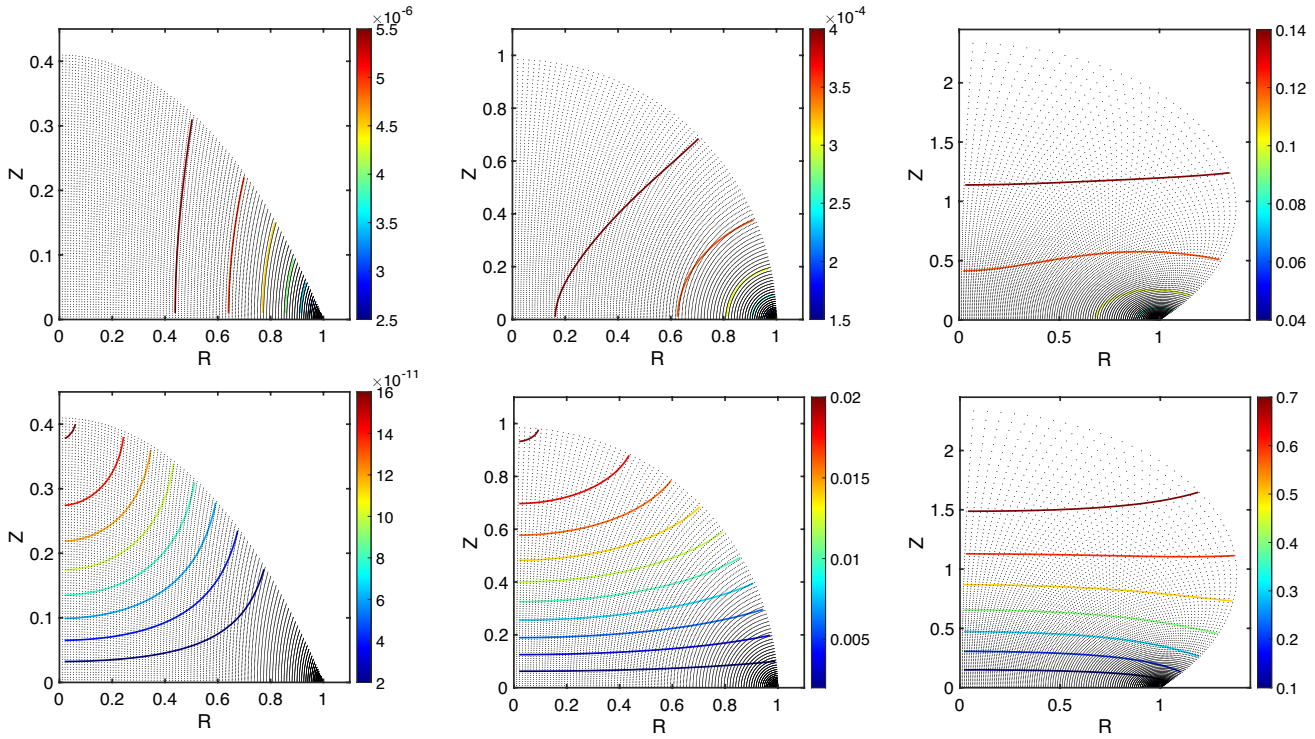

Fig. 4 Concentration profiles marking the depletion zones of species A after the chronoamperometric transients depicted in Fig. 3. The upper panels correspond to unsupported droplets (Case I); the lower panels correspond to supported droplets (Case II). Panels on the left-hand side correspond to partially wetting droplets (θ = 45°); those in the middle are for hemispherical droplets (θ = 90°); the right-hand side illustrate partially non-wetting droplets (θ = 135°). Note that the reduced timescale is different for Case I (τ = 10) and Case II (τ = 1), causing the extent of electrolysis to be different in each case: Case I (unsupported droplets; upper panels), Ω = 95.5% (θ = 45°), Ω = 95.0% (θ = 90°) and Ω = 80.3% (θ = 135°); Case II (supported droplets, lower panels): Ω = 98.9% (θ = 45°), Ω = 97.7% (θ = 90°) and Ω = 45.1% (θ = 135°). In all six examples, the numerical simulation grid employed (black circles) is overlaid by the concentration profiles

contact angle; in contrast, the same initial decay is sub-Cottrellian for the unsupported droplets and, owing to the reaction occurring at the three-phase boundary depends on the contact angle. As a result, the concentration profiles corresponding to the depletion zone are markedly different for the two cases (see Fig. 4). In Case I (unsupported droplets), the depletion zone radiates from the three-phase boundary, covering the whole droplet, so that the curvature of the concentration profiles are centred the geometry of the three-phase boundary. In unsupported, wetting droplets, seemingly one-dimensional (radial) electrolysis takes place, starting at the three-phase boundary [17]. In contrast, in Case II (supported droplets), the greater extent of electrolysis from the surface, together with the radial effect of the three-phase boundary, manifests as an "upturned collar" marking the depletion zone around the base of the droplet, for supported, wetting droplets: The curvature of the droplets is centred on the droplet apex (see Fig. 4). Note that for non-wetting droplets, the effect of convergence at the three-phase boundary singularity causes a downturn in the concentration profiles close to the electrode surface, when the state-of-conversion of the droplet is *ca.* 50%.

It follows that potential step chronoamperometry is able to provide information that discerns different droplet contact angles. However, exhaustive electrolysis for supported droplets (Case II) is required (corresponding to timescales $\tau \geq$ -2) for this to be achieved. For a millimetric droplet (a = 1 mm), and a typical redox analyte ($D \sim 10^{-5}$ cm^2 s^{-1}), this is a timescale of *ca.* 10 s, which is reasonable for electrochemical experiments. However, for unsupported droplets (Case I), there is no need for a minimum electrolysis timescale. In spite of this distinction between these two cases, these transients, nevertheless, directly evidence the potential for electrochemical goniometry. We next explore droplet voltammetry.

Figure 5 depicts linear sweep voltammograms corresponding spanning eight orders of magnitude in the dimensionless scan rate, *viz.* $0.1 \leq p \leq 10^6$, for both unsupported and supported droplets (Cases III and IV, respectively) for the three different contact angles considered for chronoamperometry. These illustrate the expected variation between thin film and diffusive effects that arise from the geometric restriction: Similar effects have been noted by Andrieux and Saveant [91] and Aoki et al. [92] for restricted planar diffusion. Whilst Laviron [93] and Shi and Anson [94] studied the

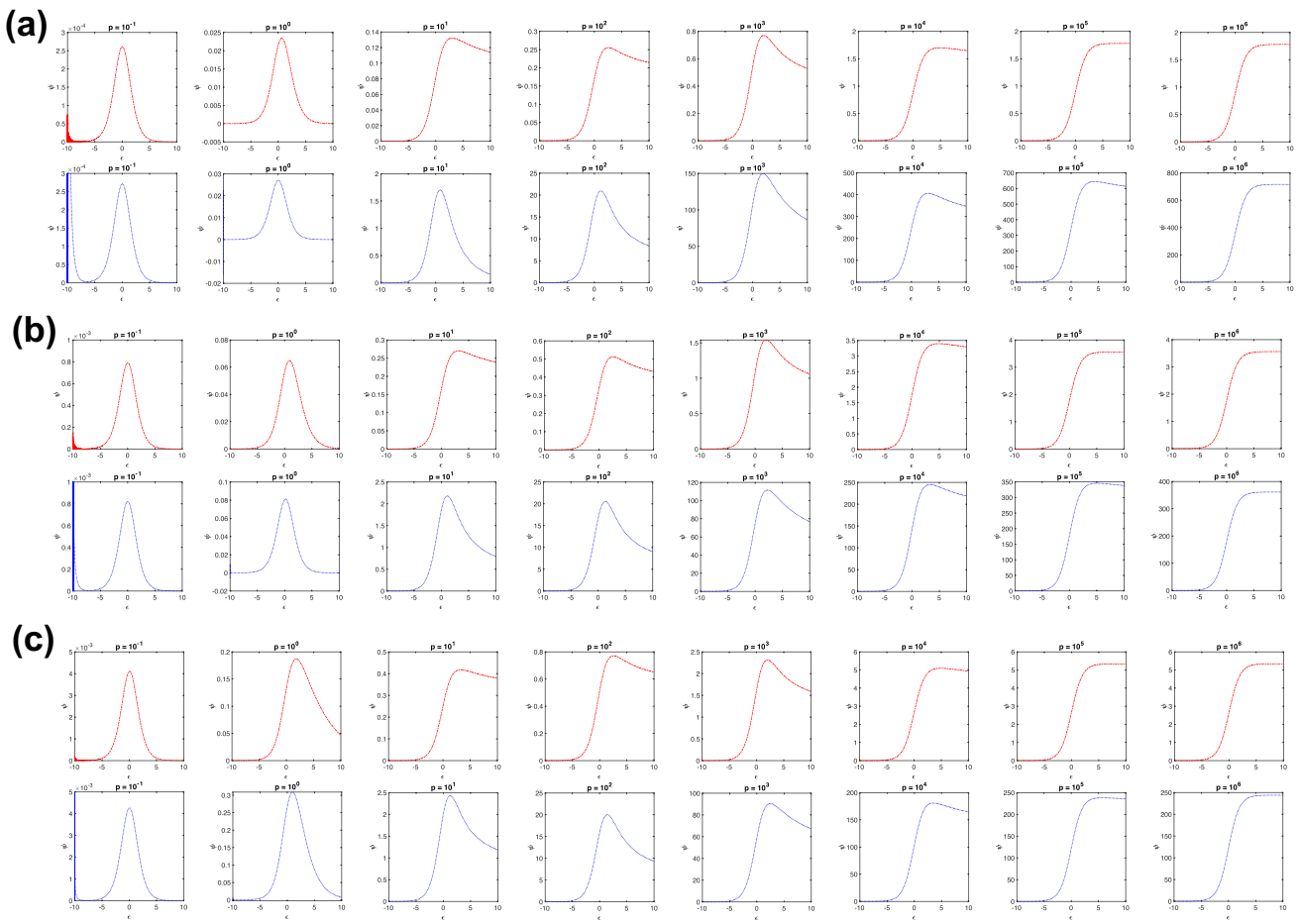

Fig. 5 Dimensionless linear sweep voltammograms for unsupported (Case III, red dot-dashed lines) and supported (Case IV, blue dotted lines) droplets, corresponding to contact angles of **a** $\theta = 45°$, **b** $\theta = 90°$ and **c** $\theta = 135°$. In each case, the dimensionless scan rate, p, is in the range $0.1 \leq p \leq 10^6$, which increases in the direction left-to-right

thin layer response of adsorbed species and supported liquid films, respectively, Amatore et al. [95, 96] demonstrated the behavioural transitions from thin film to planar diffusion and ultimately steady-state through Dahms-Ruff diffusion over an adsorbed dendrimer, spherical cap in shape.

As expected from the chronoamperometric transients reported in Fig. 3, larger currents are observed when the droplets are supported (Case IV) *c.f.* unsupported (Case III) (see Fig. 6). However, the trend in maximum current with contact angle is different for these cases: When the droplet is unsupported (Case III), an increased contact angle (increased droplet dewetting) gives rise to an increased current maximum, over all timescales. In contrast, when the droplet is supported (Case IV), this is only true for small values of $p < 10$. Above this value, a decreased contact angle (increased droplet wetting) gives rise to an increased current maximum. This crossover is also anticipated, based on the chronoamperometric results illustrated in Fig. 3, and occurs because of a change in the transport regime, as will be discussed later.

Nevertheless, in all cases, the increase in current with dimensionless scan rate occurs smoothly. The voltammetric shape changes can be explained through the comparison between the diffusion layer thickness and the droplet size. As illustrated in Fig. 6, at low values of p ($p < 1$), thin film (TF) behaviour occurs as the size of the diffusion layer, $\sim \sqrt{Dt} = \sqrt{\frac{DRT}{Fv}}$, is more massive compared with the size of the droplet, a. This causes the occurrence of the characteristic bell-shaped voltammograms, centred at the formal potential for the redox couple, $\varepsilon = 0$. These curves give peak currents that are proportional to the voltage scan rate. Increasing the value of p to unity, for which the diffusion layer size is comparable with the droplet size, causes the voltammetric peak to shift towards more positive values, whilst retaining its thin layer waveshape.

For supported droplets (Case IV), further increases in p cause the waveshape to start to resemble that for planar diffusion (PD). In this region, typically for which $\frac{\psi_p}{p} \sim 0.2232$; $\varepsilon_p \sim 1.11$; $\varepsilon_p - \varepsilon_{p/2} \sim 2.20$, an approximation

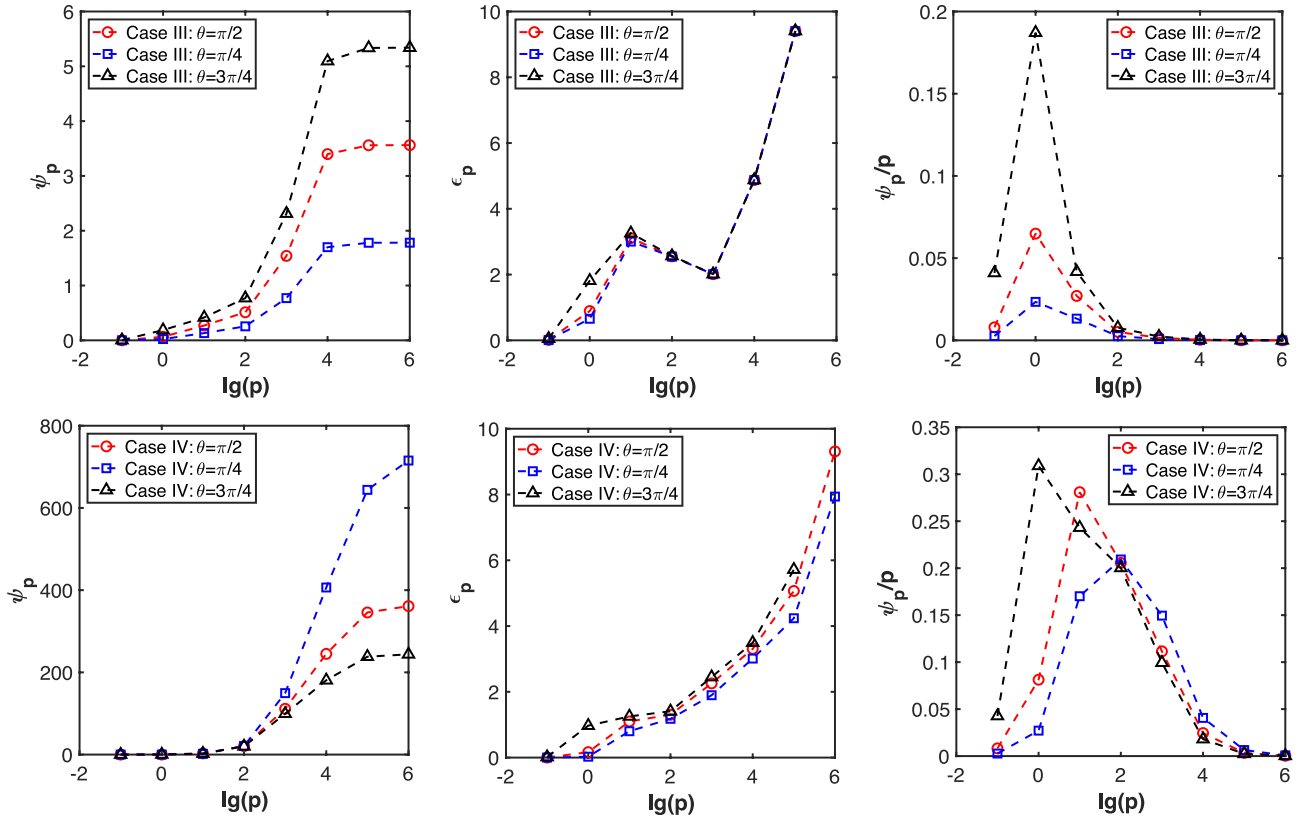

Fig. 6 Plots illustrating the change in characteristic voltammetric parameters with reduced sweep rate. The upper panels correspond to unsupported droplets (Case III); the lower panels depict the behaviour of supported droplets (Case IV). In all six cases, the results from three contact angles, corresponding to partially wetting droplets (θ = 45°, blue), partially non-wetting droplets (θ = 135°, black) and hemispherical droplets (θ = 90°, red), are given. The dashed lines are provided, so as to guide the eye

of the Randles-Ševčík equation is upheld. This regime does not occur for unsupported droplets (Case III). Instead, and as for supported droplets (Case IV) beyond the planar diffusion zone, additional increases in the value of p cause cylindrical diffusion (CD) in the droplets to occur, which leads to a zone in which the concentration profiles are at quasi-steady-state (QS).

Thus, the TF zone is characterised by the peak current increasing proportionally with scan rate, and the peak potential shifting towards higher oxidation potentials as the scan rate increases. In the PD zone, the peak potential is approximately independent of the scan rate (with $\varepsilon_p \sim 1.11$), and the peak current is directly proportional to the square-root of the scan rate. The CD zone enables supported (Case IV) and unsupported (Case III) droplets to be distinguished: In the former, the peak potential increases with scan rate and is a function of the contact angle, whilst it decreases with increasing sweep rate for the latter, irrespective of the contact angle. For both cases, $\frac{\psi_p}{p}$ decreases with increasing p. The QS region is marked by almost steady voltammograms, which are better described through their half-wave potential rather than their peak potential. In all zones, and for both cases, the three different contact angles are able to be uniquely identified, since the effect of changing the contact angle is merely to shift behaviour from one zone to the next, as evident from Fig. 6.

The occurrence of sigmoidal voltammograms at high values of p is commensurate with the previous results reported by Fulian et al. [13]. They are also in line with those reported by Myland and Oldham [15], who modelled droplets as a cones. High values of p occur whenever the voltage scan rate is large, and/or the droplet size is large, and/or the diffusion coefficient of the redox analyte is small. Such phenomena have been reported from experiments: Chen and Sato [57] employed viscous droplets to illustrate stead-state voltammograms; Compton et al. [14] reported voltammetric waveshapes changing from thin film, to diffusive, and then to quasi-steady-state as droplet deposits increased in size: a droplet of radius a ~ 1 cm at ambient temperature gives $p \sim 20{,}000$ for a scan rate of 0.1 V s^{-1} and diffusion coefficient of 10^{-6} cm^2 s^{-1}, although gravity will distort such large droplets.

Thus, having illustrated how contact angles impact on both chronoamperometric transients and voltammetric waveshapes for reversible electrode reactions, we next assess whether it is possible to infer contact angles from experimental data. Accordingly, we chose to employ a strategy of (1) estimation of contact angles from visual measurements; (2) comparison of the observed experimental current/time or current/potential data with the theory described in this section; (3) calculation of the diffusion coefficient of the redox species from (2) for the contact angle determined in (1); and (4) identification as to whether the diffusion coefficient obtained from (3) agrees with that known for the redox analyte in the bulk organic phase. This strategy is identical to knowing the diffusion coefficient and blindly determining the droplet contact angle from the electroanalytical data.

Experimental

Chemical reagents

Aqueous solutions were prepared using purified water with a resistivity greater than 18 M Ω cm obtained from an Elgastat system (Vivendi). Benzonitrile (Sigma-Aldrich) and nitrobenzene (Alfa Æsar) were purchased in > 99% purity and used as received. The electrolytes used, potassium chloride (Sigma-Aldrich) and tetra-*n*-butylammonium perchlorate (Fluka), were purchased in the highest commercially available grade. The redox reagent employed was *N*,*N*,*N*',*N*'-tetraphenyl-*para*-phenylenediamine (TPPD, 1,4-bis(diphenylamino)benzene, Sigma-Aldrich), and used as received.

Instrumentation

Electrochemical measurements were undertaken on a commercial potentiostat (Autolab PGSTAT 30, Eco-Chemie). A three electrode set-up was employed for all experiments, with a 3.0 mm (diameter) glassy carbon working electrode (BAS), a platinum or nickel spiral counter electrode and a saturated calomel reference electrode (SCE, Radiometer). The working electrode was polished with a 0.3 μm alumina slurry (Presi) on a wetted, napped polishing cloth and rinsed thoroughly with water prior to experimentation. All experiments were conducted at a temperature of 20 ± 3 °C. Droplet-modified electrodes were illuminated with a flexible light source (Prior Scientific) so that the video footage could be captured using an Olympus PV10-CB video microscope and recorded directly to a computer *via* Intervideo WindDVD Creator 2 software.

Methodology

Only supported droplets were considered. Both aqueous (containing 0.1 M KCl) and organic (containing 0.1 M $^{n}Bu_4NClO_4$) phases were mutually saturated for at least 12 h prior to experimentation. A bespoke electrochemical cell allowing for the working electrode to be positioned facing upwards was employed (see Fig. 7). The cell was filled with aqueous solutions prior to positioning a sub-microlitre organic droplet on the electrode surface via delivery through a fine soda glass capillary (prepared through controlled expansion of a molten Pasteur pipette), using a syringe pump and a three-dimensional micropositioner (Narishige). Image analysis of the liquid/liquid interface was undertaken manually from frames within the recorded video footage, comparing individual points with the equation of a truncated sphere. The error in the contact angle from these measurements was estimated as being *ca.* 5°, *viz.* approximately five times that obtained through commercial microscope goniometry.

Experimental design

A number of choices of organic phase and redox analyte were informed by preliminary experimentation or the literature, with the criteria being: (1) a redox compound that is soluble in an organic solvent, but insoluble in the aqueous phase; (2) the redox transformed material being also soluble in the organic solvent, and not expelled into the aqueous phase either through direct electrode reaction or partitioning; (3) the redox compound should not readily adsorb onto a glassy carbon electrode, but should, if possible, be electrochromic so that the optical fingerprinting the depletion zone is achievable; (4) the one-electron transformed redox material should be stable, and not decay into another species; (5) the organic phase should be easy to work with, so that separation after saturation with water is facile; and (6) the organic liquid droplet should be static throughout the redox transformation. A number of analytes, solvents and electrolytes were considered including *tert*-butylferrocene, bis(*iso*-propylcyclopentadienyl)iron, β-carotene and 5,10,15,20-tetraphenyl-21*H*,23*H*-porphine cobalt(II), together with dichloromethane and benzonitrile and tetra-*n*-butylammonium tetrafluoroborate. These were, for the main, ruled out, owing to a violation of at least one of the six rules: for example, oxidation of bis(*iso*-propylcyclopentadienyl)iron in nitrobenzene with tetrafluoroborate electrolytes led to precipitation outside the droplet, whilst changing the electrolyte anion to perchlorate caused in-droplet precipitation. In a different case, the oxidation of *tert*-butylferrocene in dichloromethane with tetrafluoroborate electrolytes enabled the observation of electrochemically induced Marangoni effects (concentration gradient induced surface tension

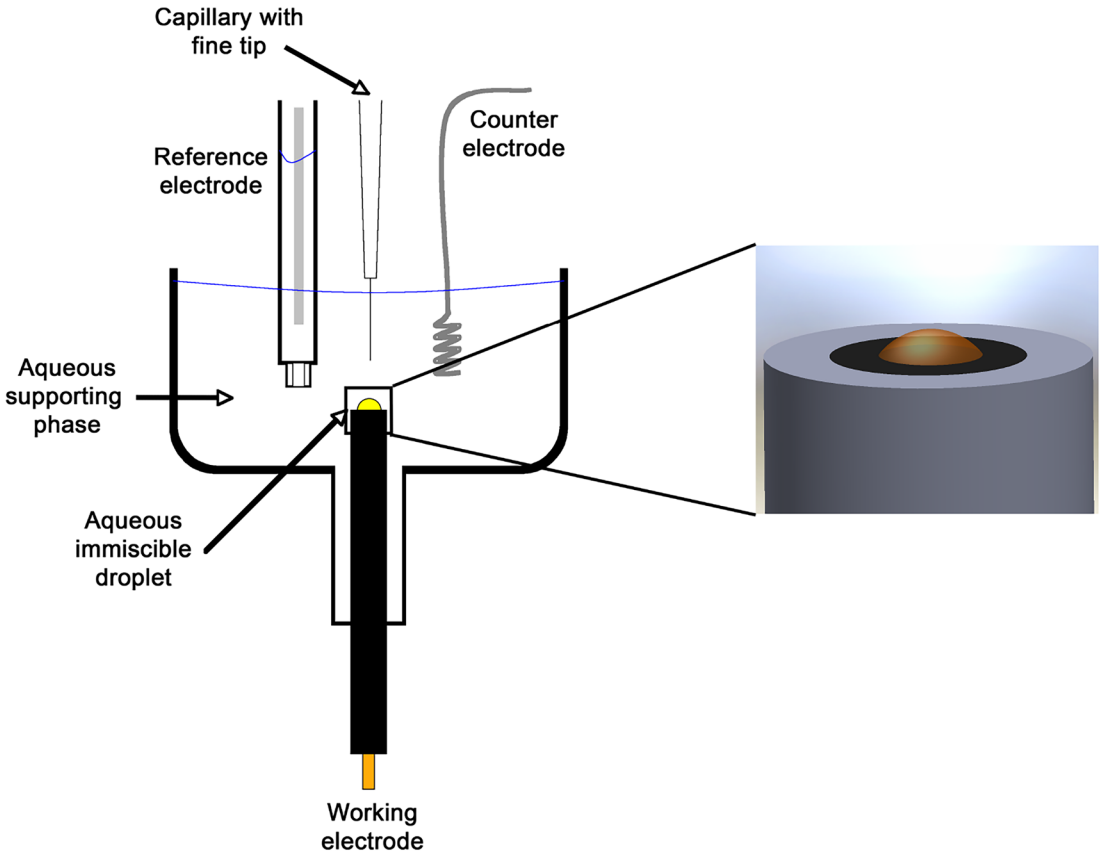

Fig. 7 Schematic diagram of the inverted working electrode arrangement employed in the experimental work reported herein

effects). Benzonitrile was kept as a solvent for TPPD, even though it was found to partially violate rule (5) in terms of ease of separation: Mixing benzonitrile and aqueous electrolytes created a suspension, which took *ca.* 60 min to settle. Accordingly, experiments were undertaken using TPPD and either nitrobenzene or benzonitrile solvents. The prior use of liquid phenylenediamines (of concentrations ~ 2 M) for studying droplet voltammetry encouraged the use of variable concentrations of TPPD to be used up to *ca.* 10 mM.

The electrolytes were chosen to provide an ideally polarised liquid/liquid interface (no exchange of ions between the two phases) in the absence of the faradaic reaction of the dissolved redox species. As a result, $^{n}Bu_4NClO_4$ was chosen for the organic phase, and KCl for the aqueous phase. Both electrolytes were kept at a concentration of 0.1 M. The use of chloride in the aqueous phase enables a robust assessment of criterion (2), since this anion is strongly hydrated, and only those electrogenerated cations that are sufficiently hydrophobic will not be ejected from the organic phase.

The timescale employed for chronoamperometric experiments was selected based on the time taken for diffusion across the longest electrode/droplet boundary distance for a millimetric-sized, hemispherical droplet. Estimates of diffusion coefficient were made for TPPD in both nitrobenzene and benzonitrile using the Wilke–Chang method [97], affording values of 6.5×10^{-6} cm^2 s^{-6} (in nitrobenzene) and 9.4×10^{-6} cm^2 s^{-1}(in benzonitrile), reflecting the relative viscosities of the two solvents. Although these values are of the order of magnitude expected [98], these estimates were confirmed through measurements made (not shown) using cyclic voltammetry at a 3.0 mm (diameter) glassy carbon electrode immersed in neat organic solvent (nitrobenzene or benzonitrile) containing 0.1 M $^{n}Bu_4NClO_4$ and 1.58 mM (nitrobenzene) or 0.94 mM (benzonitrile) TPPD, with a graphite rod counter electrode and silver wire quasi-reference electrode. These revealed that the one-electron electrode reaction at 0.1 V s^{-1} is on the reversible/quasi-reversible cusp, with a peak-to-peak separation of 109 ± 3 mV (nitrobenzene) or 92 ± 10 mV (benzonitrile). Accordingly, approximating for electrochemical reversibility, the Randles-Ševčík equation yielded diffusion coefficients for TPPD as being 2.1×10^{-6} cm^2 s^{-1} (nitrobenzene) and 3.4×10^{-6} cm^2 s^{-1} (benzonitrile). Whilst the order of the diffusion coefficients is the same as expected from the solvent viscosities, and of the correct order of magnitude, the difference in the values likely arises from, amongst other

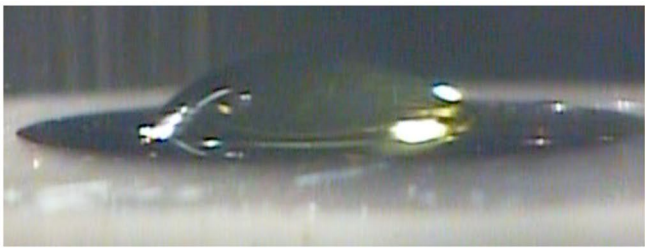

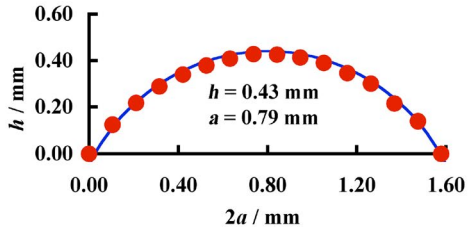

Fig. 8 Photograph (left) of a droplet of nitrobenzene containing TPPD (9.7 mM) and $^{n}Bu_4NClO_4$ (0.1 M) immobilised on the surface of a glassy carbon electrode and surrounded by a 0.1 M aqueous KCl solution. The electrode potential is 0.0 V *vs.* SCE. The plot (right) is of the co-ordinates of the liquid/liquid interface (red points) extracted manually, with the blue line being the equation of the circle that was altered to afford the best fit through minimisation of the standard mean absolute deviation between the experimental points and the theoretical line. The droplet volume was estimated as 463 ± 17 nL

things, the assumption of fast electrode kinetics. Thus, treating the diffusion coefficient as ~ 5×10^{-6} cm^2 s^{-1}, and using a droplet size of ~ 0.8 mm, the Einstein–Smoluchowski relationship for chronoamperometry, $\delta = \sqrt{\pi Dt}$, in which δ and t correspond to the characteristic length and time, respectively, affords an exhaustive electrolysis time of *ca.* 410 s. Thus, a chronoamperometric timescale of 500 s was selected so that as much of the available material within the droplet could be electrolysed. We note that this timescale is typically longer than that normally considered to preclude effects due to natural convection, and thus, it additionally serves to investigate its occurrence: Aoki has reported this for ferrocene oxidation in a nitrobenzene droplet [50]. Dick has claimed that there is limited evidence for this in water droplets bathed by 1,2-dichloroethane [99].

Results and discussion

Figure 8 depicts a supported (0.1 M $^{n}Bu_4NClO_4$) droplet of nitrobenzene containing *ca.* 10 mM TPPD freshly immobilised on the surface of a glassy carbon electrode and bathed by a 0.1 M aqueous KCl solution (pH ~ 6.5) at a potential of 0.0 V *vs.* SCE. This millimetric droplet partially wets the electrode surface, to afford a contact angle of *ca.* 57 ± 5°. As described first by Aoki and co-workers [33], this contact angle is very much different to that of a pure nitrobenzene droplet (*ca.* 90–95°), owing to electric potential effects, described by Kornyshev [36, 37]. At constant droplet volume, the interfacial tension acts to minimise the extent of the liquid/liquid interface, whilst the potential serves to maximise it. From Eq. (4), this reduction in contact angle due to the presence of the electrolyte causes an *ca.* 10% increase in the area of the liquid/liquid interface.

As illustrated in Figs. 9 and 10, the one-electron chronoamperometric transients (corresponding to *ca.* 70% droplet exhaustion) and the voltammetry are well-defined and reproducible. There is minimal change in the voltammetric waveshape after a double potential-step chronoamperometric experiment, apart from a small shift towards more positive potentials. This droplet shape is static upon electrochemical oxidation, as demonstrated in a repeat experiment (Fig. 10), for which the droplet base radius remained as a = 0.81 ± 0.05 mm, the droplet height and h = 0.38 ± 0.05 mm, giving rise to a contact angle of 51 ± 5°, irrespective of the extent of electrolysis of the droplet. This demonstrates that although different individual droplets have slightly different geometries, the droplets are not pinned: their contact angles appear to be equivalent, within experimental error.

Moreover, since there is little effect of the electrolytic oxidation process on the droplet contact angle, we suggest that, in these experiments, the electrode potential is always positive of the point-of-zero charge. Thus, any extra charge developed in the droplet through the occurrence of the faradaic reaction (producing the $TPPD^{+\bullet}$ radical cation) is balanced by the *concerted release* of $^{n}Bu_4N^{+}$ cations from the droplet to the aqueous phase. In this manner, the total number of ions inside the droplet remains constant, *viz.*:

$$\begin{aligned} \mathrm{TPPD(NB)} - \mathrm{e^-} + {}^{n}\mathrm{Bu_4N^+(NB)} + \mathrm{ClO_4^-(NB)} \\ \rightleftarrows \mathrm{TPPD^{\cdot+}(NB)} + \mathrm{ClO_4^-(NB)} + {}^{n}\mathrm{Bu_4N^+(aq)} \end{aligned} \quad (16)$$

in which NB refers to the nitrobenzene phase. The preferred expulsion of $^{n}Bu_4N^{+}$ rather than $TPPD^{+\bullet}$ is anticipated based on the Gibbs transfer energies across the liquid/liquid interface [25, 39, 77].

The occurrence of the small shift in the voltammetry after a double potential-step experiment (Fig. 10) is potentially due to effects resulting from deprotonation/protonation equilibria (since the cation radical may have a different pK_{BH+} to the parent), or to ion association effects, or to adsorption. Accordingly, experiments were undertaken in more dilute droplets, as illustrated in Figs. 11 and 12. Again, well-defined signals were obtained at TPPD concentrations of *ca.* 1.0 mM and 0.1 mM. In these experiments, the dilution causes a reduction in the mole fraction of the droplet that is oxidised, as observed through the transformation of shape the cumulative charge transients: from a "rolling" step to afford a plateau in Fig. 9, to the "sawtooth"

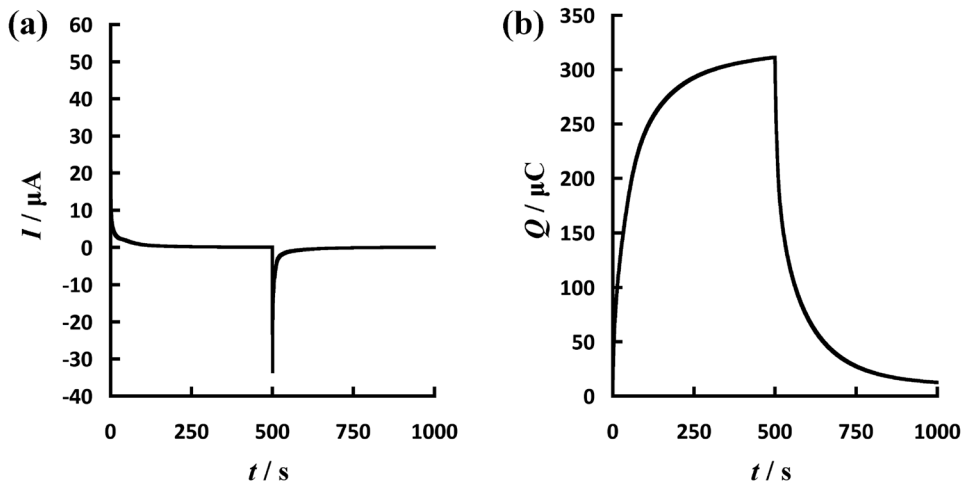

Fig. 9 Transient electrochemical behaviour of the droplet illustrated in Fig. 8: **a** chronoamperometry, with the potential of the working electrode stepped from 0.0 V (10 s) to 0.8 V *vs.* SCE; **b** cumulative charge passed, obtained through integration of the current/time transient. All experimental conditions identical to those reported in Fig. 8

shapes in Fig. 11. However, these diluted droplets give rise to minimal shifts in the voltammetry before and the single, double pulse experiments. Moreover, no adsorption peaks are observable. These indicate that little, if any, change in the drop shape or contact angle occurs. However, as shown in Fig. 12, further potential-step excursions causes the voltammograms to change shape drastically, consistent with an adsorption process occurring at the electrode surface (at *ca.* 0.2 V *vs.* SCE), and with the resulting voltammetric peak shift in the main wave, consistent with a possible ion association effect.

Comparison of experimental transients and voltammetric waveshape with the supported models developed in this work (see Fig. 13) reveal a reasonable agreement across the range of TPPD concentrations considered. The deviations between experiment and theory are likely due to the individual variations in the droplet size estimations from the multiple experiments, together with the treatment of the voltammgrams as electrochemically reversible. Non-ideal effects may also play a role [14]. The diffusion coefficients derived from the experimental data (voltammetry and chronoamperometry), $3.5 \pm 1.2 \times 10^{-6}$ cm^2 s^{-1}, are as expected for TPPD in nitrobenzene (see "Experimental" section).

Given the chronoamperometric timescale considered, this agreement in diffusion coefficients suggests that natural convection within the droplet does not play a significant role within these experiments. This must mean that the densities of the reactants and products are very similar and further point to limited ion association.

It follows that, experimentally, electrochemical goniometry can be estimated from the flowing currents, provided that the diffusion coefficient of the redox analyte used is known.

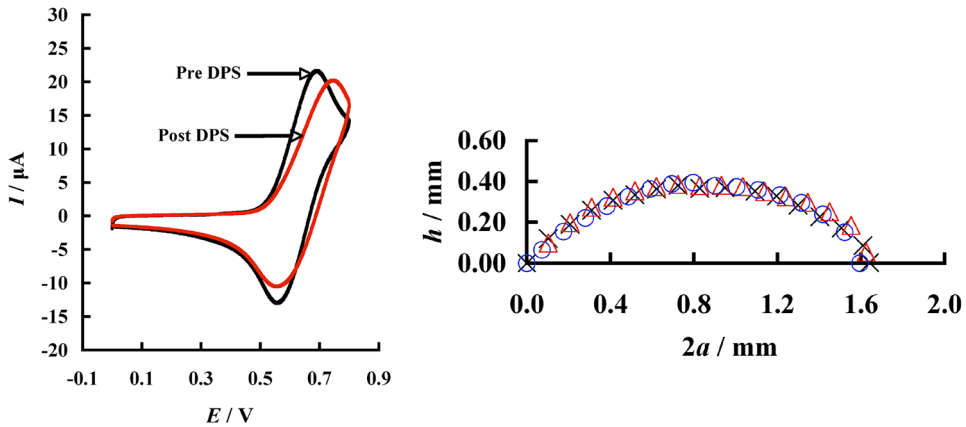

Fig. 10 Left: cyclic voltammograms (scan rate of 0.1 V s.$^{-1}$) corresponding to the one-electron oxidation of TPPD for the droplet in Figure A. The black line was recorded before undertaking the double potential-step (DPS) experiment illustrated in Fig. 9; the red line reports the results after the recording of Fig. 9. Right: Droplet profile from a repeat experiment, conditions are the same as those reported in Figs. 8 and 9: the position of the liquid/liquid interface, and how it varies with time under chronoamperometric oxidation (at 0.8 V *vs.* SCE) is illustrated using black crosses ($t = 0$ s), blue circles ($t = 250$ s) and red triangles (t = 500 s)

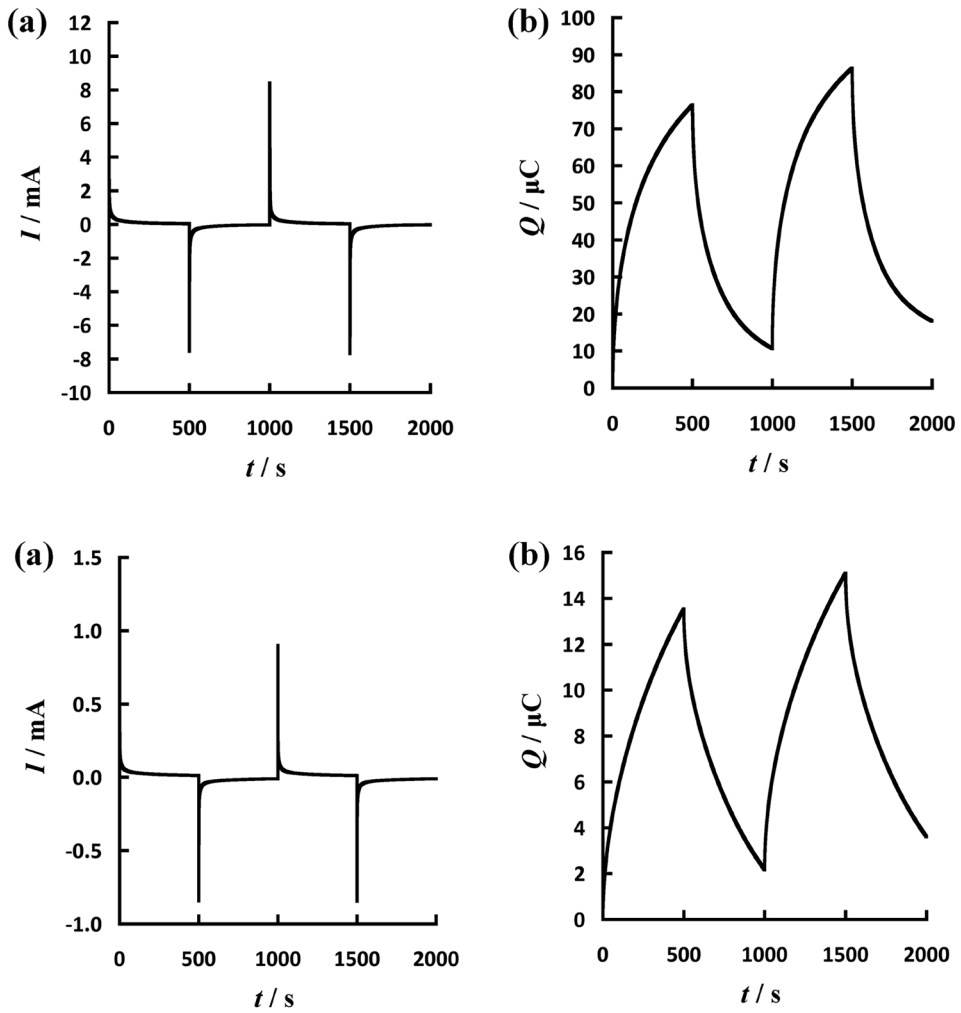

Fig. 11 Transient behaviour of diluted TPPD in nitrobenzene droplets containing 0.1 M $^{n}Bu_4NClO_4$ bathed by 0.1 M aqueous KCl. Transients were recorded as reported in Fig. 9. The TPPD concentration was 0.97 mM (upper panel) and 97 µM (lower panel). Both the chronoamperometric transient (**a**) and the cumulative integrated charge (**b**) are reported

In order to confirm this, experiments were undertaken using benzonitrile as the solvent, since this solvent affords a higher diffusion coefficient for TPPD. Figure 14 depicts a supported (0.1 M $^{n}Bu_4NClO_4$) droplet of benzonitrile containing *ca.* 9 mM TPPD freshly immobilised on the surface of a glassy carbon electrode and bathed by a 0.1 M aqueous

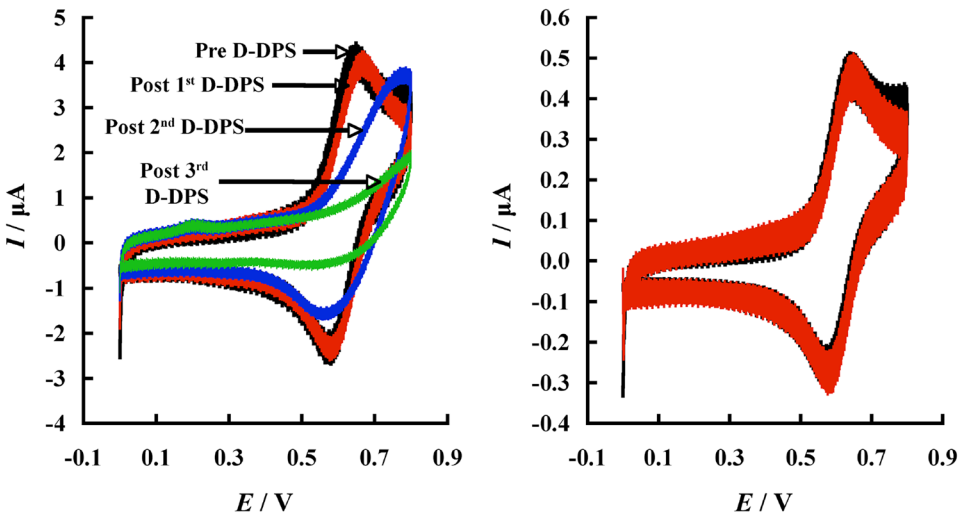

Fig. 12 Cyclic voltammograms (scan rate of 0.1 V s^{-1}) corresponding to the one-electron oxidation of TPPD droplets in Fig. 11, with a TPPD concentration of 0.97 mM (left) and 97 µM (right). The black lines were recorded before undertaking the double potential-step (DPS) experiment illustrated in Fig. 11; the red line reports the results after the recording of Fig. 11; the blue and the green voltammograms were recorded after one and two further double potential-step excursions

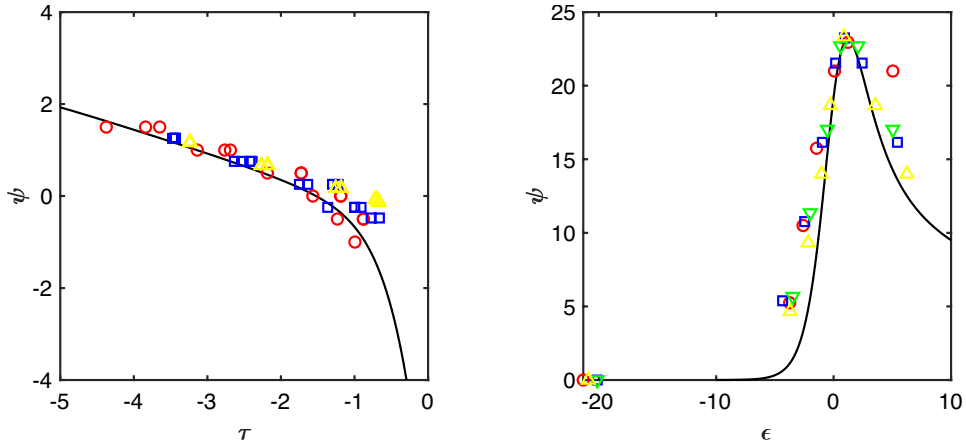

Fig. 13 Comparison between theory and experiment for the one-electron oxidation of TPPD in supported benzonitrile droplets on glassy carbon using chronoamperometry (left) and voltammetry (right). Owing to the differences in droplet sizes, theoretical lines (black) were generated assuming a = 0.81 mm and h = 0.38 mm, yielding a contact angle of *ca.* 50° (cosθ = 0.639). For voltammetry, the diffusion coefficient employed was 2.1×10^{-6} cm^2 s^{-1}, giving rise to $p = 141.2$. Experimental data correspond to TPPD concentrations of 9.7 mM (red circles), 0.97 mM (blue squares and green inverted triangles) and 97 μM (yellow triangles) for chronoamperometry (left) and voltammetry (right). The diffusion coefficient used for the fitting process was $3.5 \pm 1.2 \times 10^{-6}$ cm^2 $s.^{-1}$, with the formal potential being 0.62 ± 0.02 V *vs.* SCE. For ease of viewing, only selected points in the range 0.12–413 s (for chronoamperometry) or 0.08 – 0.77 V *vs.* SCE (for voltammetry) are depicted. The sample size of the measurements for the chronoampermetric experiments, *n*, is 3 (c_0 = 9.7 mM) and 4 (c_0 = 0.97 mM and 97 μM); for voltammetric experiments, these are *n* = 1 (c_0 = 9.7 mM and 97 μM) and 2 (c_0 = 0.97 mM)

KCl solution (pH ~ 6.5) 0.0 V *vs.* SCE. This system affords a similar contact angle to that of nitrobenzene (54 ± 5°), albeit with a slightly larger size (a = 1.00 ± 0.03 mm, h = 0.51 ± 0.02 mm). These sizes did not vary significantly during a pulsed oxidation (see Fig. 14).

Likewise, the amperometric transients and voltammograms are well-defined (Fig. 15), with the former affording a greater extent (*ca.* 80%) of electrolysis in the same time period compared with the nitrobenzene case. This is suggestive of faster transport rates in the benzonitrile droplets, as expected.

At *ca.* 10 mM TPPD concentration, although freshly immobilised droplets gave rise to little changes in the voltammetric waveshape on redox cycling over ten scans at 0.1 V s^{-1} (data not shown), a small shift occurred in the voltammograms taken before and after a double, double potential-step experiment (see Fig. 15). As with the nitrobenzene case, this shift reduced on diluting the droplets (see Figs. 16 and 17), with analogous changes occurring in the shape of the cumulative, integrated charge transients. Note that, in the case of the benzonitrile droplets, the experimental timescale for each step in potential was doubled for the case of the most diluted droplets (see Fig. 16).

In contrast with the nitrobenzene droplets, the occurrence of adsorption to the electrode is more apparent in the voltammetry, through both a small adsorption wave (at *ca.*

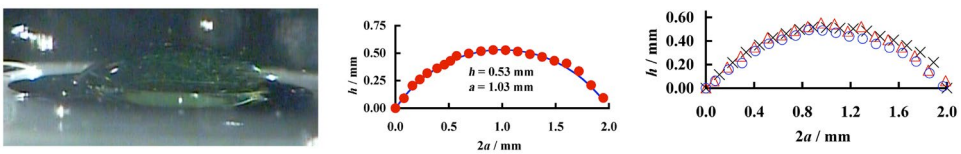

Fig. 14 Left: Photograph of a benzonitrile droplet containing TPPD (9.21 mM) and.$^{n}Bu_4NClO_4$ (0.1 M) immobilised onto a glassy carbon electrode surrounded by water containing KCl (0.1 M). Middle: plot of the co-ordinates of the liquid/liquid interface (red points) extracted manually, with the blue line being the equation of the circle that was altered to afford the best fit through minimisation of the standard mean absolute deviation between the experimental points and the theoretical line. The droplet volume was estimated as 961 ± 28 nL. Right: Droplet profile of the position of the liquid/liquid interface, and how it varies with time under chronoamperometric oxidation (at 0.8 V vs. SCE) is illustrated using black crosses (t = 0 s), blue circles (t = 250 s) and red triangles (t = 500 s)

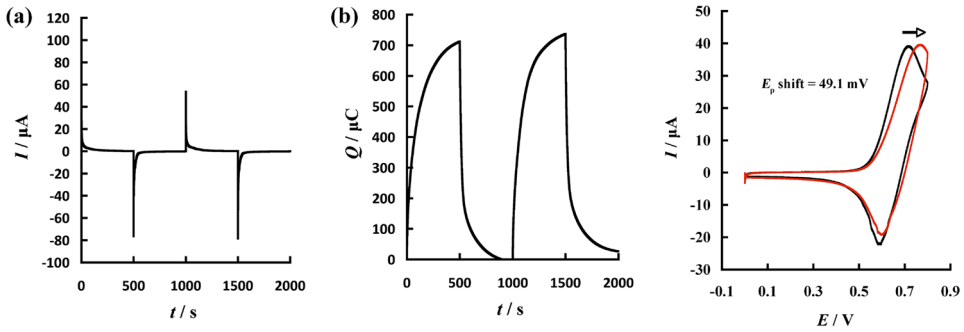

Fig. 15 Left: transient electrochemical behaviour of the droplet photographed in Fig. 14: **a** chronoamperometry, with the potential of the working electrode stepped from 0.0 V (10 s) to 0.8 V *vs.* SCE; **b** cumulative charge passed, obtained through integration of the current/time transient. Right: cyclic voltammograms (scan rate of 0.1 V s^{-1}) corresponding to the one-electron oxidation of TPPD for the droplet photographed in Fig. 14. The black line was recorded before undertaking a double, double potential-step experiment; the red line reports the results afterwards

0.2 V *vs.* SCE) and the non-systematic variations in the peak current between before and after pulsing (see Fig. 17).

There is good agreement between experimental droplet chronoamperometry with theory (see Fig. 18), giving rise to a diffusion coefficient for TPPD in benzonitrile of 3.4×10^{-6} cm^2 s^{-1}, which is in agreement with that determined experimentally (see "Experimental" section). Compared with the nitrobenzene droplets, the lower degree of variation in the data likely stems from a mixture of factors: First, there is less variation in the droplet sizes ($a = 1.00 \pm 0.03$ mm, $h = 0.51 \pm 0.02$ mm); second, fewer repeat measurements were made. Nevertheless, Figs. 13 and 18 evidence proof-of-concept for electrochemical goniometry.

This approach to spherical cap goniometry relies on the knowledge of the diffusion coefficient of the redox analyte within the droplet and the base radius of the droplet, since, through Eq. (3), the contact angle and other size parameters are related. Likewise, through the definitions of the reduced current and time (potential) variables, experimental data can be reformulated in an iterative fitting process. We note that it is only through the dependency of the current on the contact angle that occurs at the three-phase boundary that electrochemical goniometry is achievable.

Inasmuch as the above process is useful, an equally important determination is the size and shape of droplet deposits on electrodes, for which the only the contact angle is known. Here, theory (Fig. 6) can play a role through the voltammetry of a redox compound within the droplets. We note further that this approach can be extended to afford a distribution of droplet sizes that complements the inverse-space methods employed by Compton and co-workers [70, 100].

To explore this in practice, we consider the voltammetric curves of a supported TPPD/benzonitrile droplet of unknown size. This system gives an oxidative peak current that is more positive than that for nitrobenzene (Fig. 19), likely reflecting the difference in the ion transfer thermodynamics of the tetra-*n*-butylammonium cation across the liquid/liquid interface [6, 80, 101], in accordance with Eq. (16). Nevertheless, this peak current is directly proportional to the square root of the voltage sweep rate—a characteristic that is synonymous with diffusion control under the timescale considered (sweep rates of between 0.01 and 0.5 V s^{-1}, corresponding to electrochemical timescales of between 50 ms

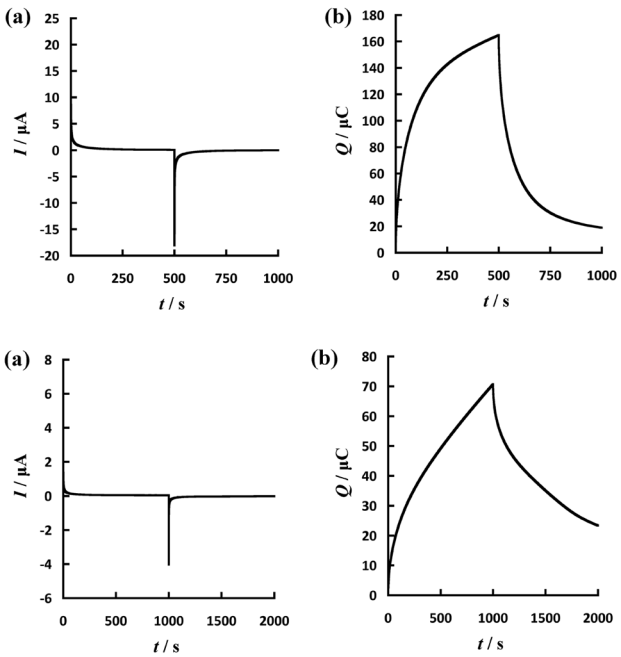

Fig. 16 Transient behaviour of TPPD in benzonitrile droplets containing 0.1 M $^{n}Bu_4NClO_4$ bathed by 0.1 M aqueous KCl. Transients were recorded as reported in Fig. 15. The TPPD concentration was 1.84 mM (upper panel) and 0.37 mM (lower panel). Both the chronoamperometric transient (**a**) and the cumulative integrated charge (**b**) are reported

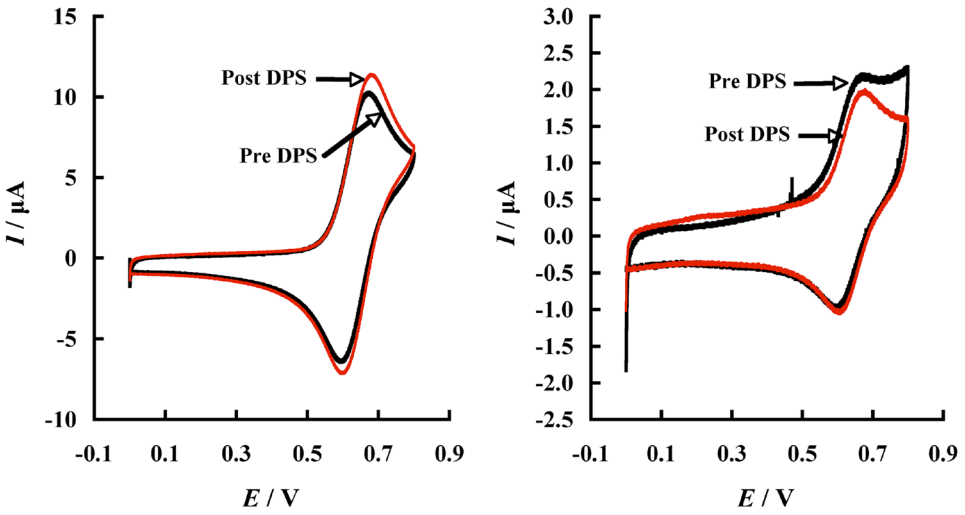

Fig. 17 Cyclic voltammograms (scan rate of 0.1 V s^{-1}) corresponding to the one-electron oxidation of TPPD droplets in Fig. 16, with a TPPD concentration of 1.84 mM (left) and 0.37 mM (right). The black lines were recorded before undertaking the double potential-step (DPS) experiment illustrated in Fig. 16; the red line reports the results afterwards

and *ca.* 2.5 s). However, both the oxidative peak potential (E_p) and the half-peak width (E_p-$E_{p/2}$) shift towards more positive values by *ca.* 40 and 24 mV decade^{-1}, respectively. Fixing the contact angle as θ = 54.0° (cosθ = 0.943) allows for simulations using reduced variables close to the PD (planar diffusion) regime (see Fig. 20). This regime is characterised by $\frac{\psi_p}{p} \sim 0.2232$; $\varepsilon_p \sim 1.11$; $\varepsilon_p - \varepsilon_{p/2} \sim 2.20$. As can be seen from Fig. 20, these characteristics, which hold for semi-infinite space, are altered by the restricted environment of the droplet. Accordingly, we employ the average value of $\frac{\psi_p}{p}$ for which $\frac{\psi_p}{p} > 0.200$, *viz.* for $20 \le p \le 200$. This gives the equivalent of the Randles-Ševčík equation for this restricted environment:

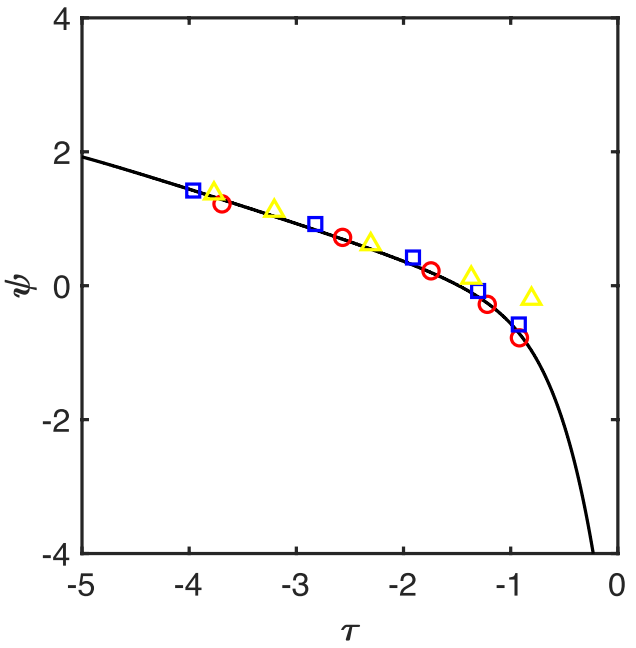

Fig. 18 Comparison between theory and experiment for the one-electron oxidation of TPPD in supported benzonitrile droplets on glassy carbon using chronoamperometry. The theoretical line (black) was generated assuming $a = 1.00$ mm and $h = 0.51$ mm, yielding a contact angle of *ca.* 54° (cosθ = 0.943). Experimental data correspond to TPPD concentrations of 9.21 mM (red circles), 1.84 mM (blue squares) and 0.37 mM (yellow triangles). The diffusion coefficient used for the fitting process was 3.4×10^{-6} cm^2 s^{-1}. For ease of viewing, only selected points in the range 0.3–440 s are depicted. Only one sample per TPPD concentration was recorded

$$\frac{\psi_p}{p} = 0.2064 \pm 0.0037 \tag{17}$$

from which the experimental plot of oxidative peak current against the square-root of the scan rate directly provides a droplet base radius, a = 0.62 ± 0.01 mm, and From Eq. (3), h = 0.32 ± 0.01 mm, values which are approximately as expected. It is noticeable that the experimental variations of both the oxidative peak potentials and half-peak widths are larger than those of determined through simulation—this is likely due to either ohmic drop or effects resulting from the electrode kinetics; the former are not considered in this work, whilst the latter are assumed to be fast in the simulations.

In returning to the theme promoted in the Introduction, we have seen that both voltammetric and chronoamperometric methods can be used for estimating the contact angle of the droplet on a conductive surface, bathed by an appropriate electrolyte solution. However, as indicated, this requires knowledge of the basal radius of the droplet, the concentration of the electroactive species within the droplet and its diffusion coefficient, together with chronoamperometric or voltammetric measurements. This empowers the algorithm given in Fig. 21 to output the contact angle through, for example, a least-squares fit between experiment and theory.

As pointed out by a Reviewer, it is important to critique this proposed method and quantify the realistic uncertainty in the resulting contact angle. To do this, we

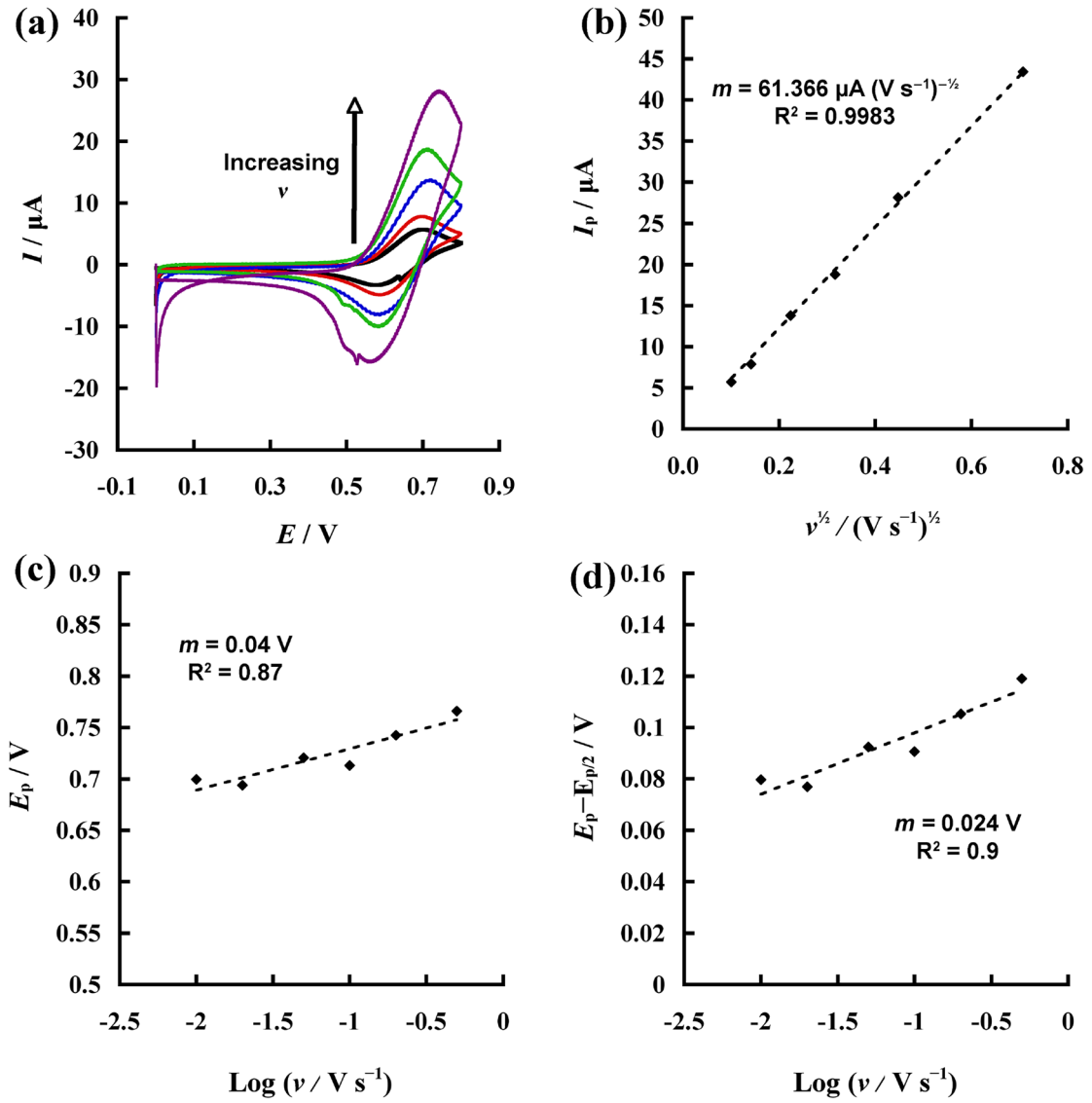

Fig. 19 **a** Cyclic voltammograms, at a glassy carbon electrode, at various scan rates, in the range 0.01–0.5 V s^{-1}, of a benzonitrile droplet containing 10.96 mM TPPD and 0.1 M $^{n}Bu_4NClO_4$, surrounded by a 0.1 M aqueous KCl electrolyte; **b** plot of oxidative peak current with the square-root of the scan rate; **c** variation of the peak oxidative current with scan rate; **d** dependence of the half-peak width on the experimental timescale. In (**b**)–(**d**), *m* refers to the gradient of the straight line, with R^2 being the coefficient of determination

need to consider the relative uncertainties in each of the measured variables. Thus, for currents, we use a relative error of 5%, since this is the error in the determination of the peak or plateau current that is used classically for constructing kinetic zone diagrams [102]. For droplet size, since this is obtained through photography, we, and others [99], typically use the visible diameter of the electrode as a scale (3.0 mm), giving a relative uncertainty of (100 × 0.05/3.0) ~ 2%. It is also important to recognise that any pinning of the contact angle will impact on this parameter so that multiple experiments with a fresh droplet each time should be undertaken. The relative uncertainty in the diffusion coefficient is as much as ~ 10% (Wilke–Chang approximation), or ~ 1% (*viz.* 100 × 0.05/5.0, for measurements accurate to two significant figures). Measurement uncertainty in the concentration of redox analyte is a function of the tolerance of the glassware used and the balance employed: for 25 mL of solution, with a 1.0 mM concentration of analyte (of molar mass 500 g mol^{-1}), a four-figure balance affords an uncertainty of 0.4% in the mass, and a 0.1% or 0.2% uncertainty in the glassware used to make the solution. This gives a relative error in concentration of *ca.*

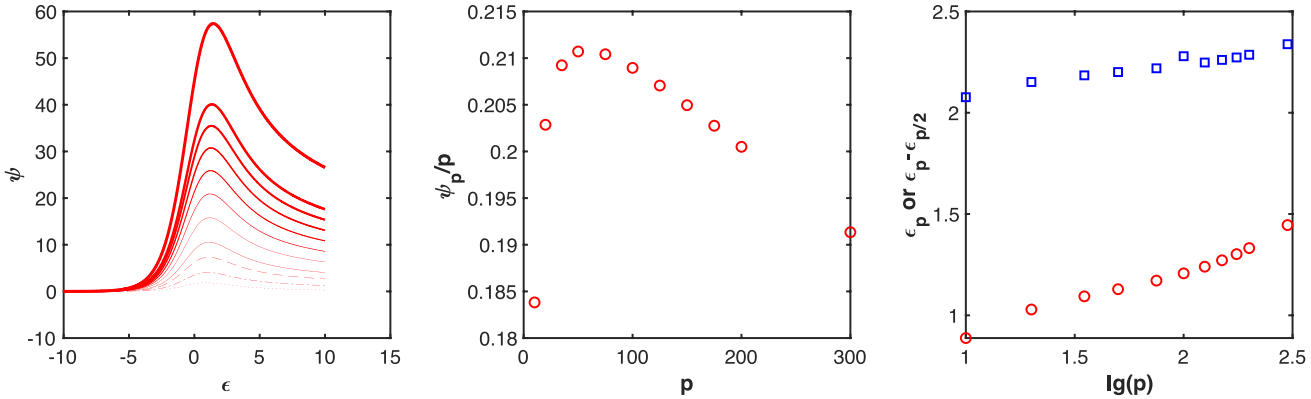

Fig. 20 Left: Simulated voltammograms for an electrochemically supported liquid droplet on an electrode surface with contact angle θ = 54.0° (cosθ = 0.943) containing a redox compound of known diffusion coefficient, with (from top to bottom) $p = 300$, 200, 175, 150, 125, 100, 75, 50, 35, 20 and 10, M: variation of ψ_p/p against p illustrating the approximately planar diffusion region for $20 \le p \le 200$. Right: variation of the oxidative peak potential (red circles) and half-peak width (blue squares) with timescale

1%. Hence, the overall uncertainty [103] in the estimation of the dimensionless current is between 9 and 18%. As indicated in Eqs. (12) and (14), this is the uncertainty in the contact angle. The uncertainty in the Fourier number (for both chronoamperometry and voltammetry) is approximately the same 5–14%. Thus, to a best realistic estimation, the error in the contact angle determined through Fig. 21 is ~ 10%. Although this is typically larger than those from commercial goniometry systems, we note that it can reduce, by almost half, if careful and skilful practice is employed for measuring currents, determining electrode size and preparing solutions of the electroactive species.

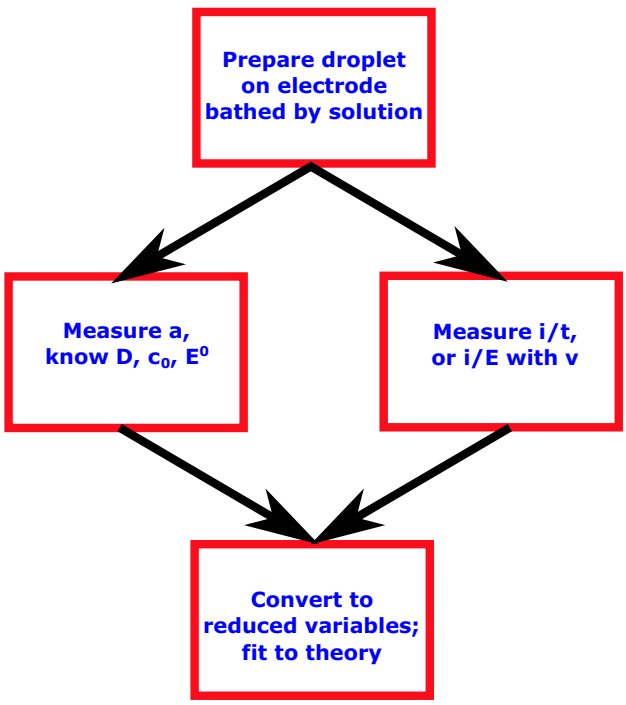

Fig. 21 Flow diagram illustrating the proposed algorithm for electrochemical goniometry

Conclusions

In this work, we have seen that electrochemical tools and techniques can be utilised for monitoring the size and shape of liquid droplets covering a conductive surface and bathed by a different, immiscible liquid. This has been verified through experimental measurements for two different droplet solvents bathed by aqueous solution. The reactivity at the triple phase boundary empowers a quantitative relationship between the contact angle and the observed current. However, practical systems need to be designed carefully, so as to ensure that transport within the droplet is well defined, and there are no opportunities for chemical instabilities to arise that may affect the transport regime. In the experimental systems considered, limited effects due to ion association and natural convection have been observed.

Despite the restricted nature of the droplet-modified electrode, a key feature of the reactivity is that when the droplets contain a level of supporting electrolyte, there is a zone (p ~ 10–100) in which planar diffusion occurs. This causes the confined environment of the droplet to behave as though it is semi-infinite space above the circular disc of the droplet base. This is a profound change, since defined relationships between current and scan rate (in voltammetry) or time (in chronoamperometry) exist, and their experimental observation is a function of the droplet volume, $p = \sqrt[3]{\frac{3}{\pi}V_{cap}}\sqrt{\frac{Fv}{RT}}\sqrt[3]{\frac{(1+cos\theta)^2}{sin\theta(2+cos\theta)}}$, Thus, for a droplet of just sub-microlitre volume (e.g. 920 nL) filled with an aqueous electrolyte and immobilised on a glassy carbon electrode under ambient conditions, the contact angle of 127°

and analyte diffusion coefficient of 5×10^{-6} cm^2 s^{-1}, which are typical conditions [99], voltammetry within the very limited, but typical [99], range of sweep rates from 0.01 V s^{-1} to 1 V s^{-1}, is essentially in the planar diffusion zone. This is why finite element simulations in two-dimensional space, but using one-dimensional equations for transport and flux [20], appear to work for the voltammetry of such droplets; we note that the use of the classical analytical expressions for one-dimensional transport would be both faster for analysis, and more accurate, [104] assuming diffusion-only transport occurs.

Acknowledgements We thank the following for useful discussions of the ideas contained in this work: Professor Frank Marken, Professor Richard Compton, Professor Uwe Schröder, Professor Lembit Nei, Professor Christian Amatore, Professor Emmanuel Maisonhaute, Professor Bernd Schöllhorn, Dr. Yann Bouret, Dr. Stephane Arbault, Professor Irina Svir and Dr. Oleksandr Oliynyk. We thank Dr. François Mavré, Dr. Yan Zhou and Dr. Laetitia Testut for helping with some preliminary experiments. We thank the Engineering and Physical Sciences Research Council (grant number: EP/G020833/1), The Leverhulme Trust (grant number: SAS/30105) and The University of Hull for funding, with hosted, visiting professorships for JDW supported by Equipe de NanoSystèmes Analytiques (NSysA, ENSCPB/Université de Bordeaux I) and Laboratoire d'Electrochimie Moléculaire (LEM, Université de Paris VII: Denis Diderot). It is a pleasure to acknowledge the improvements made to this manuscript by two anonymous reviewers.

Declarations

Conflict of interest The authors declare no competing interests.

References

1. Shaw DJ (1992) Introduction to colloid and surface chemistry, 4th edn. Butterworth-Heinemann, Oxford
2. Hunter RJ (1993) Introduction to modern colloid science. Oxford University Press, Oxford
3. de Gennes P-G, Brochard-Wyart F, Quere D (2004) Capillarity and wetting phenomena: drops, bubbles, pearls, waves. Springer, New York
4. von Baeyer HC (2000) The lotus effect. The Sciences 40:12
5. Stauber JM, Wilson SK, Duffy BR (2015) Evaporation of droplets on strongly hydrophobic substrates. Langmuir 31:3653
6. Scholz F, Kormorsky-Lovrić Š, Lovrić M (2000) A new access to Gibbs energies of transfer of ions across liquid/liquid interfaces and a new method to study electrochemical processes at well-defined three-phase junctions. Electrochem Commun 2:112
7. Banks CE, Davies TJ, Hignett Evans RG, Wain AJ, Lawrence NS, Wadhawan JD, Marken F, Compton RG (2003) Phys Chem Chem Phys 5:4053 see for example
8. Scholz F, Schröder U, Gulaboski R, Doménech-Carbó A (2015) Electrochemistry of immobilised particles and droplets: experiments with three-phase electrodes, 2nd edn. Springer, Heidelberg For a more in-depth review
9. Kauffman PJ, Dick JE (2023) Single liquid aerosol nano-impact electrochemistry accessing the droplet/air interface. Environ. Sci. Nano. 10:1744
10. Fietkau N, Chevallier FG, Jiang L, Jones TGJ, Compton RG (2006) Voltammetric sizing of a sphere. ChemPhysChem 7:2162
11. Feess H, Wendt H (1980) Performance of electrolysis with two-phase electrolyte: the trickle electrode for the electrochemical conversion of substances with low solubility in aqueous electrolytes with special respect to electrochemical extraction processes. J Chem Tech Biotechnol 30:297
12. Lovrić M (1999) Diffusion from a three-phase junction into a hemispherical droplet. Electrochem Commun 1:207
13. Fulian Q, Ball JC, Marken F, Compton RG, Fisher AC (2000) Voltammetry of electroactive oil droplets: Part I – numerical modelling for three mechanistic models using the dual reciprocity finite element method. Electroanalysis 12:1012
14. Ball JC, Marken F, Fulian Q, Wadhawan JD, Blythe AN, Schröder U, Compton RG, Bull SD, Davies SG (2000) Voltammetry of electroactive oil droplets: Part II – comparison of experimental and simulation data for coupled ion and electron insertion processes and evidence for microscale convection. Electroanalysis 12:1017
15. Myland JC, Oldham KB (2000) Modelling reversible cyclic voltammetry at the one-dimensional junction established by three phases: an organic liquid containing a neutral electroactive solute, an aqueous electrolyte solution and an electronic conductor. Electrochem Commun 2:541
16. Terui N, Nakatani K, Kitamura N (2000) Kinetic analysis of electrochemically induced ion transfer across a single microdroplet/water interface. J Electroanal Chem 494:41. Although this work does not examine droplets with an active three-phase boundary, it highlights effects owing to the restricted spherical cap geometry, and illustrates several problems associated with the discretisation of the space for use in in a finite difference numerical simulation
17. Aoki K, Tasakorn P, Chen J (2003) Electrode reactions at submicron oil/water/electrode interfaces. J Electroanal Chem 542:51
18. Lovrić M, Scholz F (2003) Modelling cyclic voltammograms of simultaneous electron and ion transfer reactions at a conic film three-phase electrode. J Electroanal Chem 540:89
19. Amatore C, Oleinick A, Svir I (2005) Diffusion within nanometric and micrometric spherical-type domains limited by nanometric ring or pore active interfaces: Part I – conformal mapping approach. J Electroanal Chem 575:103
20. Reyes-Morales J, Glasscott MW, Pendergast AD, Goines S, Dick JE (2022) The oxidation of ferrocene in sessile toluene macro- and microdroplets: an opto-electrochemical study. J Electroanal Chem 905:115922. For the use of finite element methods using-COMSOL Multiphysics for the modelling of the voltammetry ofdroplets see for example
21. Rayner D, Fietkau N, Streeter I, Marken F, Buckley BR, Page PCB, del Campo J, Mas R, Muñoz FX, Compton RG (2007) Electrochemical investigation of hemispherical microdroplets of N, N-didodecyl-N', N'-diethylphenylenediamine immobilised as regular arrays on partially-blocked electrodes: a new approach to liquid/liquid voltammetry. J Phys Chem C 111:9992
22. Dharmaraj K, Nasri Z, Kahlert H, Scholz F (2018) The electrochemistry of DPPH in three-phase electrode systems for ion transfer and ion association studies. J Electroanal Chem 823:765

23. Marken F, Webster RD, Bull SD, Davies SG (1997) Redox processes in microdroplets studied by voltammetry, microscopy and ESR spectroscopy: oxidation of N, N, N', N'-tetrahexyl-para-phenylenediamine deposited on solid electrode surfaces and immersed in aqueous electrolyte solution. J Electroanal Chem 437:209
24. Schröder U, Compton RG, Marken F, Bull SD, Davies SG, Gilmour S (2001) Electrochemically driven ion insertion processes across liquid/liquid boundaries: neutral *versus* ionic redox liquids. J Phys Chem B 105:1344
25. Lledo-Fernandéz C, Hatay I, Ball MJ, Greenway GM, Wadhawan J (2009) Electrogenerated chemiluminescence at droplet-modified electrodes: towards biphasic pK_a measurement *via* proton-coupled electron transfer at liquid/liquid interfaces. New J Chem 33:749
26. Glasscott MW, Dick JE (2020) Visualising phase boundaries with electrogenerated chemiluminescence. J Phys Chem Lett 11:4803
27. Donten M, Bak E, Gniadek M, Stojek Z, Scholz F (2008) Three-phase electrochemistry with a hanging drop of water-insoluble liquid: precipitation of decamethylferricenium species as a marker of ion transfer route. Electrochim Acta 53:5608
28. Colón-Quintana GS, Vannoy KJ, Renault C, Voci S, Dick JE (2022) Tuning the three-phase microenvironment geometry promotes phase formation. J Phys Chem C 126:20004
29. Wadhawan JD, Evans RG, Banks CE, Wilkins SJ, France RR, Oldham NJ, Fairbanks AJ, Wood B, Walton DJ, Schroder U, Compton RG (2002) Voltammetry of electroactive oil droplets: electrochemically induced ion insertion, expulsion and reaction processes at microdroplets of N, N, N', N'-tetraalkyl-para-phenylenediamines (TRPD, R = n-butyl, n-hexyl, n-heptyl and n-nonyl). J Phys Chem B 106:9619
30. Davies TJ, Wilkins SJ, Compton RG (2006) The electrochemistry of redox systems within immobilised water droplets. J Electroanal Chem 586:260
31. Clarke TB, Dick JE (2022) Preferential electroreduction at the oil/water/conductor interface. J Phys Chem Lett 13:3338
32. Donten M, Stojek Z, Scholz F (2002) Electron transfer-ion insertion electrochemistry at an immobilised droplet: probing the three-phase electrode reaction zone with a Pt disc microelectrode. Electrochem Commun 4:324
33. Tasakorn P, Chen J, Aoki K (2002) Voltammetry of a single oil droplet on a large electrode. J Electroanal Chem 533:119
34. Quentel F, Mirčeski V, L'Her M, Mladenov M, Scholz F, Elleouet C (2005) Comparative study of the thermodynamics and kinetics of ion transfer across the liquid/liquid interface by means of three-phase electrodes. J Phys Chem B 109:13228
35. Weatherly CKT, Ren H, Edwards MA, Wang L, White HS (2019) Coupled electron- and phase-transfer reactions at a three-phase interface. J Am Chem Soc 141:18091
36. Monroe CW, Daikhin LI, Urbakh M, Kornyshev AA (2006) Principles of electrowetting with two immiscible electrolytic solutions. J Phys Condens Matter 18:2837
37. Kornyshev AA, Kucernak AR, Marinescu M, Monroe CW, Sleightholme AES, Urbakh M (2010) Ultra-low voltage electrowetting. J Phys Chem C 114:14885
38. Zhang G, Walker M, Unwin PR (2016) Low-voltage voltammetric electrowetting of graphite surfaces by ion intercalation/deintercalation. Langmuir 32:7476
39. Lomax DJ, Kant P, Williams AT, Patten HV, Zou Y, Juel A, Dryfe RAW (2016) Ultra-low voltage electrowetting using graphite surfaces. Soft Matter 12:8798
40. Cousens NEA, Kucernak ARJ (2017) Reversible ultralow voltage liquid/liquid electrowetting without a dielectric layer. Faraday Discuss 199:63
41. Halls JE, Altalhi AA, de Abreu FC, Goulart MOF, Wadhawan JD (2012) Concentration-dependent diffusion coefficients of *tert*-butylferrocene within dodecyltrimethylammonium chloride/brine liquid crystals. Electrochem Commun 17:41
42. Wadhawan JD, Wain AJ, Kirkham AN, Walton DJ, Wood B, France RR, Bull SD, Compton RG (2003) Electrocatalytic reactions mediated by N, N, N', N'-tetraalkyl-1,4-phenylenediamine redox liquid microdroplet-modified electrodes: chemical and photochemical reactions in, and at the surface of, femtolitre droplets. J Am Chem Soc 125:11418
43. Wain AJ, Lawrence NS, Greene PR, Wadhawan JD, Compton RG (1867) Reactive chemistry *via* the redox switching of microdroplets of 4-nitrophenyl nonyl ether in the presence of aqueous electrolytes. Phys Chem Chem Phys 2003:5
44. Halls JE, Wadhawan JD (2012) Photogalvanic cells based on lyotropic nanosystems: towards the use of liquid nanotechnology for personalised energy sources. Energy Environ Sci 5:6541
45. Amatore C, Berthou M, Herbert S (1998) Fundamental principles of electrochemical Ohmic heating of solutions. J Electroanal Chem 457:191
46. Moore MR, Vella D, Oliver JM (2021) The nascent coffee ring: how solute diffusion counters advection. J. Fluid Mech. 920:A54. See for example
47. Selman JR, Newman J (1971) Free-convection mass transfer with a supporting electrolyte. J Electrochem Soc 118:1070
48. Novev JK, Compton RG (2018) Natural convection effects in electrochemical systems. Curr Opinion Electrochem 7:118
49. Cai B, Ge J, Zhu F, Gao Y, Jiao S (2023) Understanding natural convection in low-concentration electrochemical systems: validation of the convection modes. J Electroanal Chem 950:117865
50. Aoki K, Satoh M, Chen J, Nishiumi T (2006) Convection caused by three-phase boundary reactions. J Electroanal Chem 595:103
51. Everett DH (1972) Manual of symbols and terminology for physicochemical quantities and units, Appendix II definitions, terminology and symbols in colloid and surface chemistry. Pure Appl. Chem. 31:577. cited by the IUPAC Gold Book: https://goldbook.iupac.org/terms/view/C01290 (Acessed 30 Mar 2024)
52. Murray MD, Darvell BW (1990) A protocol for contact angle measurement. J Phys D Appl Phys. 23:1150
53. Lebedev NN, Silverman RA, (translator) (1965) Special functions and their applications. Prentice-Hall Inc, Englewood Cliffs, NJ, USA
54. Evans LA, Thomasson MJ, Kelly SM, Wadhawan JD (2009) Electrochemical determination of diffusion anisotropy in molecularly structured materials J Phys Chem C 113:8901. See for example
55. Aoki K, Osteryoung JG (1981) Diffusion-controlled current at the stationary finite disc electrode: theory. J Electroanal Chem 122:19. with correction provided in idem., ibid., 1984, 160, 335.
56. Shoup D, Szabo A (1982) Chronoamperometric current at finite disc electrodes. J Electroanal Chem 140:237
57. Chen J, Sato M (2004) Steady-state current at oil/water/electrode interfaces using ion-insoluble polydimethylsiloxane droplets. J Electroanal Chem 572:153
58. Kätelhön E, Compton RG (2015) Testing and validating electroanalytical simulations. Analyst 140:2592
59. Marken F, Blythe A, Compton RG, Bull SD, Davies SG (1999) Sulphide accumulation and sensing based on electrochemical processes in microdroplets of N^1-[4-(dihexylamino)phenyl]-N^1, N^4, N^4-trihexyl-1,4-phenylenediamine. Chem Commun 1823
60. Wain AJ, Wadhawan JD, Compton RG (2003) Electrochemical studies of vitamin K_1 microdroplets: electrocatalytic hydrogen evolution. ChemPhysChem 4:974
61. Rees NV, Wadhawan JD, Klymenko OV, Coles BA, Compton RG (2004) An electrochemical study of the oxidation of 1,3,4-tris[4-[(3-methylphenyl)phenylamino]phenyl]benzene. J Electroanal Chem 563:191
62. Wain AJ, Wadhawan JD, France RR, Compton RG (2004) Biphasic redox chemistry of α-tocopherol: evidence for electrochemically induced hydrolysis and dimerization on the surface of, and

within, femtolitre droplets immobilised onto graphite electrodes. Phys Chem Chem Phys 6:836
63. Katif N, MacDonald SM, Kelly AM, Galbraith E, James TD, Lubben AT, Opałło M, Marken F (2008) Electrocatalytic determination of sulphite at immobilised microdroplet liquid/liquid interfaces: the EIC' mechanism. Electroanalysis 20:469
64. Collins AM, Zhang XH, Scragg JJ, Blanchard GJ, Marken F (2010) Triple-phase boundary photovoltammetry: resolving rhodamine B reactivity in 4-(3-phenylpropyl)-pyridine microdroplets. ChemPhysChem 11:2862
65. Marken F, Wadhawan JD (2019) Multiphase methods in organic electrosynthesis. Acc Chem Res 52:3325
66. Wadhawan JD, Compton RG, Marken F, Bull SD, Davies SG (2001) Photoelectrochemcially driven processes at the N, N, N', N'-tetrahexylphenylenediamine microdroplet/electrode aqueous triple interface. J Solid State Electrochem 5:301
67. Ulmeanu S, Lee HJ, Fermin DJ, Girault HH, Shao Y (2001) Voltammetry at a liquid/liquid interface supported on a metallic electrode. Electrochem Commun 3:219
68. Davies TJ, Banks CE, Nuthakki B, Rusling JF, France RR, Wadhawan JD, Compton RG (2002) Surfactant-free emulsion electrosynthesis *via* power ultrasound: electrocatalytic formation of carbon-carbon bonds. Green Chem 4:570
69. Wadhawan JD, Wain AJ, Compton RG (2003) Electrochemical probing of photochemical reactions inside femtolitre droplets confined to electrodes. ChemPhysChem 4:1211
70. Davies TJ, Brookes BA, Compton RG (2004) A computational and experimental study of the cyclic voltammetry response of partially blocked electrodes, part III: interfacial liquid/liquid kinetics of aqueous vitamin B_{12s} with random arrays of femtolitre microdroplets of dibromocyclohexane. J Electroanal Chem 566:193
71. Chevallier FG, Davies TJ, Klymenko OV, Jiang L, Jones TGJ, Compton RG (2005) Influence of the block geometry on the voltammetric response of partially blocked electrodes: application to interfacial liquid/liquid kinetics of aqueous vitamin B_{12s} with random arrays of femtolitre microdroplets of dibromocyclohexane. J Electroanal Chem 580:265
72. Davies TJ, Garner AC, Davies SG, Compton RG (2004) Cyclic voltammetry at microdroplet modified electrodes. A comparison of the reaction of vicinal dibromides with vitamin B_{12s} at the liquid/liquid interface with the corresponding homogeneous process: evidence for polar solvent effects at the liquid/liquid interface. J Electroanal Chem 570:171
73. Davies TJ, Garner AC, Davies SG, Compton RG (2005) Insights into the role of the liquid/liquid interface in biphasic reactions: the reaction of vitamin B_{12s}(aq) with vicinal dibromides (oil). ChemPhysChem 6:2633
74. Horn JJ, Watson A, Lewis M, McCreedy T, Wadhawan JD (2008) Reaction between L-cysteine and 10-methylphenothiazine cation radical released from droplet-modified electrodes. Electrochem Commun 10:1384
75. Marken F, Compton RG, Goeting CH, Foord JS, Bull SD, Davies SG (1998) Anion detection by electro-insertion into N, N, N', N'-tetrahexylphenylenediamine (THPD) microdroplets studied by voltammetry. EQCM and SEM techniques, Electroanalysis 10:821
76. Marken F, Blythe AN, Wadhawan JD, Compton RG, Bull SD, Aplin RT, Davies SG (2001) Voltammetry of electroactive liquid redox systems: anion insertion and chemical reactions in microdroplets of *para*-tetrakis(6-methoxyhexyl)phenylenediamine, *para*- and *meta*-tetrahexylphenylenediamine. J Solid State Electrochem 5:17
77. Marken F, Compton RG, Goeting CH, Foord JS, Bull SD, Davies SG (2001) Fast electrochemical triple interface processes at boron-doped diamond electrodes. J Solid State Electrochem 5:88
78. Marken F, Hayman CM, Page PCB (2002) Chromate and dichromate electro-insertion processes into a N, N, N', N'-tetraoctylphenylenediamine redox liquid. Electrochem Commun 4:462
79. Marken F, Hayman CM, Page PCB (2002) Phosphate and arsenate electro-insertion processes into a N, N, N', N'-tetraoctylphenylenediamine redox liquid. Electroanalysis 14:172
80. Schröder U, Wadhawan J, Evans RG, Compton RG, Wood B, Walton DJ, France RR, Marken F, Page PCB, Hayman CM (2002) Probing thermodynamic aspects of electrochemically driven ion-transfer processes across liquid/liquid interfaces: pure *versus* dilute redox liquids. J Phys Chem B 106:8697
81. Wadhawan JD, Evans RG, Compton RG (2002) Voltammetric characteristics of graphite electrodes modified with microdroplets of *n*-butylferrocene. J Electroanal Chem 533:71
82. Stott SJ, McKenzie KJ, Mortimer RJ, Hayman CM, Buckley BR, Page PCB, Marken F, Shul G, Opałło M (2004) Liquid/liquid ion-transfer processes at the dioctylphosphoric acid (N, N-didodecyl-N', N'-diethylphenylenediamine)/water (electrolyte) interface at graphite and mesoporous T_iO2 substrates. Anal Chem 76:5364
83. Marken F, McKenzie KJ, Shul G, Opałło M (2005) Ion transfer processes at 4-(3-phenylpropyl)-pyridine/aqueous electrolyte/electrode triple-phase boundary systems supported by graphite and by mesoporous TiO_2. Faraday Discuss 129:219
84. Watkins JD, Bull SD, Marken F (2009) Ultrasound mobilisation of liquid/liquid/solid triple phase boundary redox systems. J Phys Chem C 113:15629
85. Vagin MY, Karyakin AA, Vuorema A, Sillanapää M, Meadows H, del Campo FJ, Cortina-Puig M, Page PCB, Chan YH, Marken F (2010) Coupled triple phase boundary processes: liquid/liquid generator-collector electrodes. Electrochem Commun 12:455
86. Zhang XH, Paddon CA, Chan YH, Page PCB, Fordred PS, Bull SD, Chang HC, Rizvi N, Marken F (2009) Voltammetric antioxidant analysis in mineral oil samples immobilised into boron-doped diamond micropore array electrodes. Electroanalysis 21:1341
87. Halls JE, Wadhawan JD (2011) Biphasic voltammetry of N, N, N', N'-tetraphenyl-para-phenylenediamine microdroplets, microparticles and microparticle suspensions. Electroanalysis 23:997
88. Du Chateau P, Zachmann DW (1986) Schaum's outline of theory and problems of partial differential equations. McGraw-Hill, New York See for example
89. Britz D, Oldham KB, Østerby O (2009) Strategies for damping the oscillations of the alternating direction implicit method of simulation of diffusion-limited chronoamperometry at disc electrodes. Electrochim Acta 54:4822
90. Amatore C, Svir I (2003) A new and powerful approach for simulation of diffusion at microelectrodes based on overlapping subdomains: application to chronoamperometry at the microdic. J Electroanal Chem 557:75
91. Andrieux CP, Savéant J-M (1980) Electron transfer through redox polymer films. J Electroanal Chem 111:377
92. Aoki K, Tokuda K, Matsuda H (1983) Theory of linear sweep voltammetry with finite diffusion space. J Electroanal Chem 146:417
93. Laviron E (1979) General expression of the linear potential sweep voltammogram in the case of diffusionless electrochemical systems. J Electroanal Chem 101:19
94. Shi C, Anson FC (1998) A simple method for examining the electrochemistry of metalloporphyrins and other hydrophobic reactants in thin layers of organic solvents interposed between graphite electrodes and aqueous solutions. Anal Chem 70:3114
95. Amatore C, Bouret Y, Maisonhaute E, Goldsmith JI, Abruña HD (2001) Ultrafast voltammetry of adsorbed redox active dendrimers with nanometric resolution: an electrochemical microtome. ChemPhysChem 2:130
96. Amatore C, Bouret Y, Maisonhaute E, Goldsmith JI, Abruña HD (2001) Precise adjustment of nanometric scale diffusion layers

within a redox dendrimer molecule by ultrafast cyclic voltmmetry: an electrochemical nanometric microtome. Chem Eur J 7:2206
97. Wilke CR, Chang P (1955) Correlation of diffusion coefficients in dilute solutions. Am Inst Chem Eng J 1:264
98. Evans RG, Klymenko OV, Hardacre C, Seddon KR, Compton RG (2003) Oxidation of N, N, N', N'-tetraalkyl-para-phenylenediamines in a series of room temperature ionic liquids incorporating the bis(trifluoromethylsulfonyl)imide anion. J Electroanal Chem 556:179
99. Vannoy KJ, Dick JE (2022) Oxidation of L-cysteine by electrogenerated ferricyanide in microlitre droplets. Langmuir 38:11892
100. Davies TJ, Brookes BA, Fisher AC, Yunus K, Wilkins SJ, Greene PR, Wadhawan JD, Compton RG (2003) A computational and experimental study of the cyclic voltammetric responses of partially blocked electrodes, Part II: randomly distributed and overlapping blocking systems. J Phys Chem B 107:6431
101. Gulaboski R, Mirčeski V, Komorsky-Lovrić Š, Lovrić M (2020) Three-phase electrodes: a simple and efficient tool for the analysis of ion transfer processes across liquid/liquid interfaces – twenty years on. J Solid State Electrochem 24:2575
102. Saveant JM, Su KB (1984) Homogeneous redox catalysis of electrochemical reactions, Part VI zone diagram representation of the kinetic regimes. J. Electroanal. Chem. 171:341. See for example
103. Miller JN, Miller JC (2005) Statistics and chemometrics for analytical chemistry, 5th edn. Pearson, Harlow See for example
104. Cutress IJ, Dickinson EJF, Compton RG (2010) Analysis of commercial general engineering finite element software in electrochemical simulations. J Electroanal Chem 638:76